Multi-axial damage and failure models for thick composite lugs under static and cyclic loading

Master of Science Thesis in Lightweight Structures

JEAN-MICHEL RAMEAU

Supervisor: Dipl.-Ing. Marco Hoffmann, Airbus Group Innovations
Examiner: Prof. Dr.-Ing. Dan Zenkert, KTH Royal Institute of Technology

Stockholm, September 2015

Abstract

The thesis deals with quasi-static and fatigue simulations of thick composite lugs subjected to three-dimensional stress states. This includes damage prediction of hybrid laminates made of GRFP and CRFP containing unidirectional and woven fabric plies.

Focus lies on the development of a progressive damage model in fatigue which accounts for stiffness and strength degradations. Two methods based on Puck's failure criterion are proposed to predict failure of unidirectional plies: one for plane stress analysis and and the other which takes out-of-plane damage into account.

Virtual testing in FEM is conducted in quasi-static and fatigue analysis on thick composite lugs subjected to uni-axial loading. Damage, strength and life predictions are then compared with experimental results to validate the numerical models under investigations.

Keywords: fibre-reinforced composite, multi-axial, quasi-static, fatigue, damage, Puck's criterion

Zusammenfassung

Masterarbeit im Bereich Leichtbaustruktur

In der vorliegenden Arbeit wird die Berechnung der Festigkeit von dickwandigen Lochleibungslaminaten im Faserverbundwerkstoffen unter dreidimensionalen Spannungszuständen untersucht. Nichtlineare Materialverhalten von Hybridlaminaten in CFK und GFK werden für Unidirektionalfaserlagen und Gewebelagen berücksichtigt.

Der Schwerpunkt liegt auf der Entwicklung von progressiven Versagensmodellen unter der Berüsichtigung von Restfestigkeit und Reststeifigkeit des Materials. Zwei Modellierungsmethoden nach Puck-Kriterium zur Vorhersage des Versagens in UD-Lagen werden vorgeschlagen: eine Degradierungstechnik für ebene Spannungszustände und ein mehrachsiges Modell.

Numerische Simulationen mit der Finite-Elemente-Methode werden in Statik- und Ermüdungsanalyse an dickwandigen Lochleibungslaminaten unter einachsiger Belastung durchgeführt. Beschädigungen, Festigkeiten und Ermüdungslebensdauer werden dann mit experimentiellen Daten verglichen, um die numerischen Methoden zu validieren.

Schlagwörter: Faserverbundwerkstoff, mehrachsige Spannung, statische Berechnung, Ermüdung, Puck-Kriterium, Schaden

Contents

List of Figures

List of Tables

Nomenclature

Acronyms

2D	two-dimensional
3D	three-dimensional
CLD	Constant life diagram
CRFP	Carbon-fibre reinforced plastic
FEM	Finite element method
FF	Fibre failure
FRC	Fibre reinforced composite
GRFP	Glass-fibre reinforced plastic
IFF	Inter fibre failure
ILS	Interlaminar shear
IP	Integration point
MFB	Master fracture body
MPC	Multi-point constraint
S-N	Stress-Life
UCS	Ultimate compressive stress
UD	Unidirectional
UMAT	User material behaviour subroutine
UTS	Ultimate tensile stress

Coordinate Systems

r, ϕ	Cylindrical coordinate system of the laminate, ϕ being an angle inclined to the x-axis in the (x0y) plane
x, y, z	Global coordinate system of the laminate, x being longitudinal direction, z through-thickness direction
x_1, x_2, x_3	Coordinate system of a UD lamina, x_1 being fibre-parallel, x_3 in through-thickness direction
x_1, x_n, x_t	Coordinate system of an action plane, x_1 being fibre-parallel
$x_\parallel$, $x_\perp$	Cylindrical coordinate system of a UD lamina, $x_\parallel$ being fibre-parallel

Greek symbols

ϵ	Strain	[-]
η	Stiffness degradation factor	[-]
ν	Poisson's ratio	[-]
ϕ	Inclined angle from the x-axis in the (x0y) plane	[rad]
ψ	Direction of the resultant shear in an action plane	[rad]
σ	Stress	[MPa]
τ	Shear stress	[MPa]
θ	Orientation of an action plane	[rad]

Latin symbols

d	Damage variable	[-]
E	Young's modulus	[GPa]
F	Force	[kN]
f_E	Stress exposure	[-]
G	Shear modulus	[GPa]
K	Stiffness matrix	
m_{σ_f}	Magnification factor for matrix stresses	[-]
n	Number of loading cycles	[-]
N_f	Number of loading cycles until failure	[-]
p	Inclination parameter for the fracture curve from Puck's theory	[-]
R	Stress ratio	[-]
R^A	Fracture resistance of the action plane	[MPa]
R_i	Strength of the material in i direction	[MPa]
E	Elastic modulus	[MPa]

Chapter 1

Introduction

The use of composite materials is becoming more important in the construction of aerospace structures with a clear aim to reduce the overall weight and cost of a vehicle. Analysis and test methods have been extensively developed for thinner structures where the behaviour is rather well understood. There is moreover an increasing demand for the design of attachments with thick laminates which requires consequently suitable analysis methods to consider out-of-plane loads. In this context, the use of thick composite lugs is increasingly becoming interesting and represents an area of research in the development of helicopter components. Innovative concepts developed by Airbus Helicopters are for instance leading to a special interest in integrating thick composite lugs into the helicopter. The design of such components brings crucial needs in improving numerical methods to estimate the strength under static as well as under fatigue loading conditions.

Previous work has been conducted to predict the strength of thick composite laminates under static load by FEM simulations [1]. Some research has also been done on fatigue analysis in the wind energy sector. However an important lack remains in the estimation of the fatigue life of thick composite laminates and particularly for aerospace applications.

The presented thesis has its emphasis on investigations to predict the strength of thick composite lugs under static and pulsating tensile loading by FE analysis. A review of current numerical models is first carried out to present suitable failure criteria and material degradation models for fibre reinforced composites. Analysis methods implemented for static and fatigue analyses are presented and analysed with the objective to generate a design guideline for composite lugs.

Chapter 2

The NEROBA programme

2.1 Motivation

The rotor system is an area of great interest in the design of helicopters. Due to aerodynamic forces applied on the blades and inertial forces, the structural parts of the rotor are subjected to high static and dynamic loadings. In this context, the design of rotor led to an extensive use of composite materials with the clear aim to reduce the overall weight of an helicopter. For these reasons, the 4^{th}-class EC135 helicopter developed by Airbus Helicopters is equipped with thick attachments in fibre reinforced composites to transfer stresses between the blades and the rotor mast.

The programme ATR3 (acronym for Advanced Technology Rotor) was launched with the purpose of developing an economic and efficient production of main rotor blades in composites along with the need for integration of folding rotor blades for military applications. Multiple concepts have been studied from the present rotor system of the helicopter EC135 depicted in Figure 2.1 and result in the separation of the present part into a composition of flexelement, control cuff and blade. The flexelement and the control cuff are connected to the blade by two bolts to make blade folding possible. The new design philosophy aims to reduce the complexity of the production by separating aerodynamic parts of the blade. The loading in the junction of the rotor head is considerably reduced through the clear decomposition of flexelement and blade parts. The connection between those elements can be then guaranteed by a composite lug. This choice leads to a flatter structure in comparison to the use of a loop resulting in a higher aerodynamic efficiency.

As part of the NEROBA programme, acronym for "Neue Rotorblatt-Bauweisen" (english: new rotor blade construction), static and dynamic strengths are investigated as well as critical load and failure modes under the influences of boundary conditions, geometric dimensions, types of materials and stacking sequences. The dimensions of the specimens are carefully chosen with respect to the needs of the

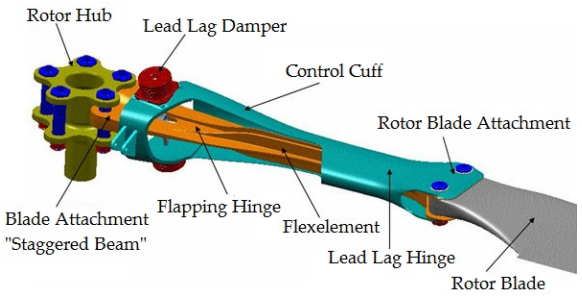

Figure 2.1: Rotor system design of ATR-3 (from www.airbushelicopters.com)

rotor concept ATR3. The study covers investigations on the structural behaviour of thick composite lugs which connect the blades with the rotor mast.

2.2 Characteristics of the composite lug

2.2.1 Specimen geometry

The composite lug under study is a thick attachment made of fibre-reinforced plastic (FRP) which contains one hole at each extremity. The different specimens used for this study share the same geometric characteristics according to Figure 2.2.

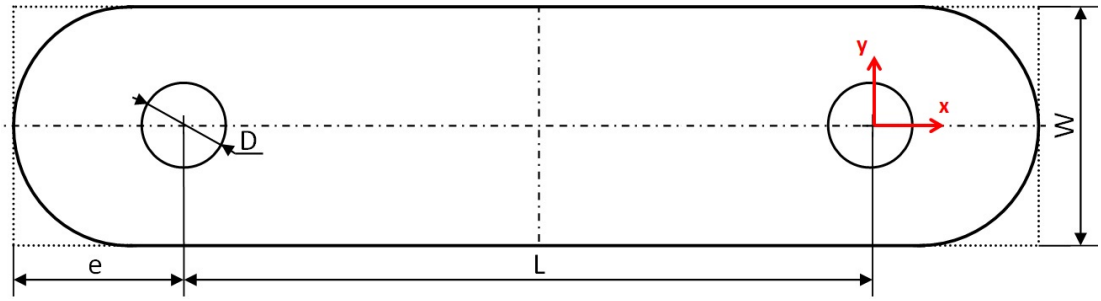

Figure 2.2: Schematic representation of the lug

2.2.2 Laminate layup of specimens

The strength of the lug is investigated for different materials and stacking sequences of composite plies. Three different symmetric laminate compositions used refer to the specimens 1, 3 and 4. The numbering of the lug specimens are kept the same as in the NEROBA programme.

Specimen 1

The first lug specimen is composed of composite material made of an epoxy matrix reinforced with R-glass fibres. The laminate is assembled with unidirectional (UD) plies oriented in 0°, 90° and ±45°. The layup contains more than 50% of 0°-plies and little proportion of 90°-plies.

Specimen 3

Specimen 3 corresponds to an E-glass/epoxy composite material composed of UD and woven fabric layers with different orientations and with more than 50% of 0° UD-plies and less than 10% of 0°/90° fabric plies.

Specimen 4

The composite lug of type 4 is a hybrid laminate made of E-glass/epoxy as well as carbon/epoxy. It is composed of more than 50% of 0° UD-plies and more than 30% of ±45° fabric plies.

2.3 Experimental tests

Components of rotor blades are subjected to three essential types of loads [1]:

1. Bending moment due to the flapping motion produced by the asymmetric lift distribution as depicted in Figure 2.3
2. Loading from the lagging motion of the rotor blades caused by the Coriolis forces induced by the flapping motion
3. Centrifugal force $F = m\omega^2/R$

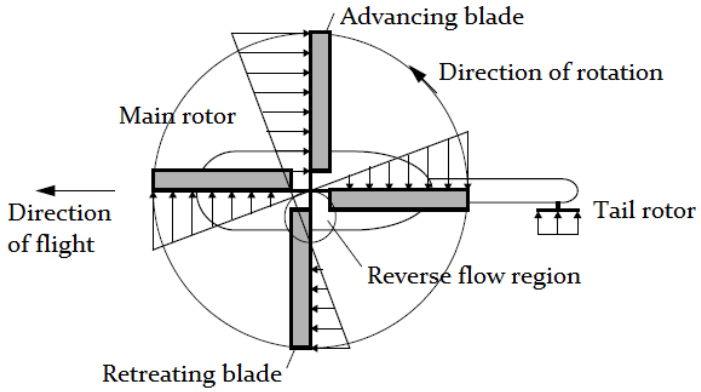

Figure 2.3: Asymmetric lift distribution in forwarding flight (adapted from [2])

In the NEROBA programme, the structural behaviour of the composite lugs is studied through an experimental test programme. Specimens of the composite lugs

are tested under static and cyclic longitudinal loading in order to simulate effects of the centrifugal force. The structural behaviour of the lug due to lagging and flapping motions is also studied in the test programme, but is not covered by the present study.

The test programme includes experiments of composite materials with the view to characterise the fatigue strength of individual plies. Tests are also conducted on composite lugs and used here to validate the numerical models under investigation aiming to predict failure of the component under static and fatigue loading conditions.

2.3.1 Strength of composite materials

A set of experimental tests has been conducted to evaluate the strength of the unidirectional glass-fibre reinforced plastics (E-glass/epoxy) under constant cyclic loading. Fatigue strengths in fibre direction and in interlaminar shear (ILS) are estimated via a 3-point-bending test of a 0° UD laminate beam.

Fatigue strength in fibre direction

Under cyclic bending conditions, the outer surfaces of the laminate specimen are subjected to an induced normal stress in the direction of the fibres. The beam for the test is chosen long and thin in order to have interlaminar shear stress negligible in comparison to longitudinal normal stress. Interlaminar shearing is hence supposed not to give any contribution in the fatigue of the material composite. S-N curves of the fatigue failure are a function of the maximum longitudinal stress in the exterior surface of the tensile part of the beam. They describe the fatigue strength of the composite in fibre failure for the stress ratios $R = \frac{\sigma_{min}}{\sigma_{max}} = [0.5, 0.2, 0.05, -0.5, -1]$ with σ_{min} and σ_{max} respectively the maximum stress and the minimum stress located at the failed point.

Fatigue strength under interlaminar shear

Similarly to the previous test, the interlaminar shear fatigue strength of unidirectional and woven fabric glass/epoxy composites is predicted through a 3-point-bending test. For the UD laminates, fibres are oriented at 0° whereas the woven fabric laminates have a $[0°, 90°, \pm 45°]_{ns}$ lay-up. Here the beam is dimensioned to be short and thick so that the fatigue damage of the materials is dominated by interlaminar shear failure via delamination. A S-N curve for the stress ratio $R = -1$ is determined based on the values of the highest ILS stress causing delamination in the middle fibre layer of the beam.

2.3.2 Failure of composite lugs

In the experimental test of lugs, the specimens are bolted and loaded by fixing one bolt and pulling the opposite one as seen in Figure 2.4. The numbering of Figure 2.4

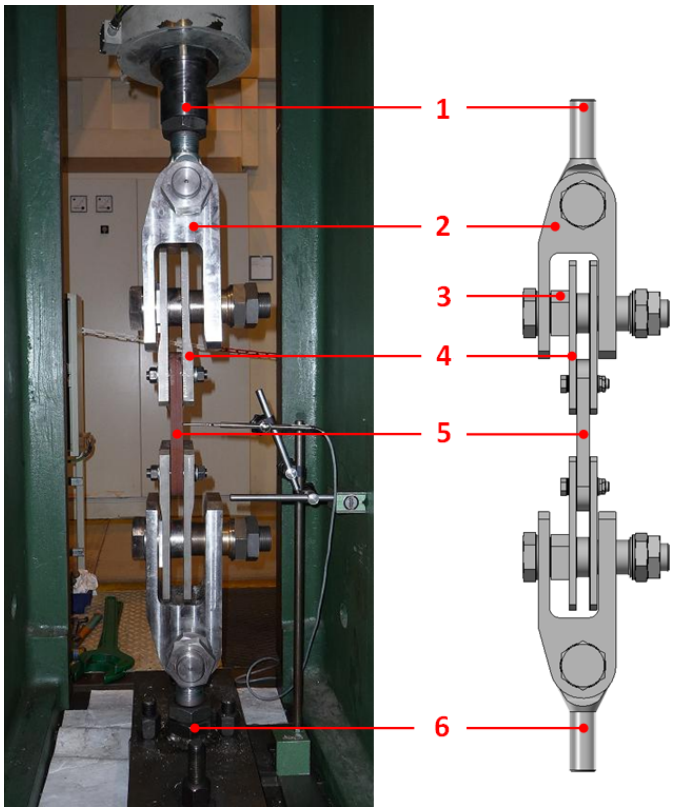

Figure 2.4: Test facility in the NEROBA test programme (from [1])

indicates the following descriptions:

1. Connection to the hydraulic cylinder for the introduction of a tensile force
2. Triple clamp for transferring the force from the hydraulic cylinder to the flange plates through the bolts
3. Spacer
4. Flange plate
5. Lug specimen
6. Lower fixation

The presence of the flange plates in the test programme is designed to take into consideration the contact with the attachment from the flexelement and the control cuff to the aerodynamic areas of the blades.

A Teflon-Liner is put on the upper surface of the lug to avoid damaging the specimen due to the contact to the flange plates as seen in Figure 2.5. The bushes separating the specimen and the bolts are glued in the holes of the lug. The numbering in

Figure 2.5: Lug specimen used for the NEROBA programme

Figure 2.5 refers to the following description:

1. Composite lug
2. Teflon-Liner
3. Bush

Chapter 3

Review of literature

Fatigue degradation within fibre reinforced composites is of very different nature from the initiation to the growth compared to that of metallic materials. The bearing-capacity of composite structures is less deteriorated under cyclic loading condition compared to metallic components. Fatigue of composites exhibits a complex behaviour where various degradation mechanisms such as matrix microcracking and fibre breakage come into play. Review of experimental observations and methods relative to damage and failure of composite laminates is conducted. Regarding the high interest of developing a numerical tool to predict fatigue life of thick composite lugs, the present section focuses particularly on the fatigue analysis of composite laminates.

3.1 Structural behaviour of fibre reinforced composites under cyclic loading

The prediction of fatigue strength in composite lugs requires a good understanding of the fatigue behaviour of laminates. The present section clarifies basic aspects of degradation and failure mechanisms in UD and woven fabric composites under cyclic loading conditions as well as effects on the stiffness and the strength of structures.

The fatigue behaviour of composite materials is influenced by diverse factors.

- load magnitude and direction
- type of fibre
- type of matrix
- stacking sequence
- environmental conditions (eg. temperature and moisture)

3.1.1 Fatigue of fibre reinforced composites

Early research on the fatigue performance at the beginning of the 1970's demonstrated that higher modulus carbon fibre composites had an excellent fatigue behaviour with nearly flat stress-life curves and a low strength degradation rate [3]. However lower modulus glass fibre composites had a relatively poor fatigue performance with steeper stress-life curves and higher strength degradation rates. Damage mechanisms in UD composites depend greatly on the relations between static failure strains and the matrix resin fatigue strain limits. The fatigue damage mechanisms in UD composites consist of fibre damage which occurs catastrophically and matrix and interfacial damage evolving progressively [3].

Talreja [4] proposed a description of degradation mechanism of composites under on-axis cyclic loading where fibre breakage, interfacial debonding and matrix cracking come into play. The author depicted the behaviour of unidirectional composites for tensile fatigue by constructing schematic fatigue-life diagrams where strain is chosen instead of stress as seen in Figure 3.1. As shown in the figure, the horizontal

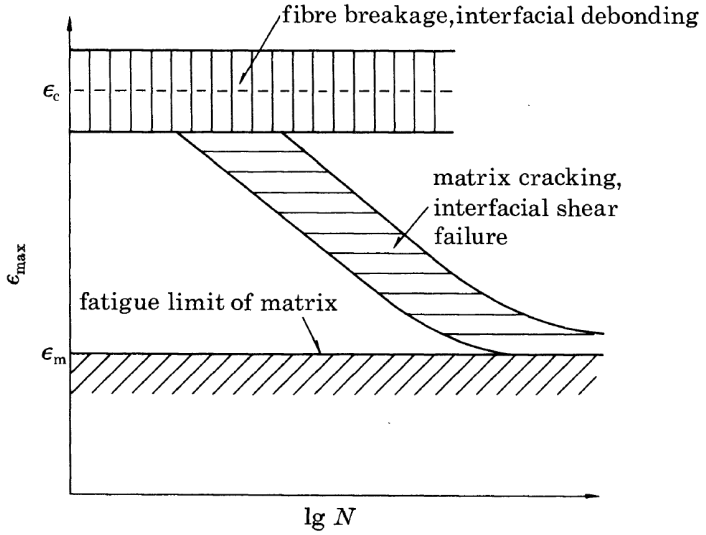

Figure 3.1: Fatigue-life diagram for unidirectional composites under loading parallel to fibres (from [4])

band centred about the composite fracture strain ϵ_c corresponds to fibre breakage and the resulting interfacial debonding. The next region is shown as a sloping band between the lower bound of the fibre-breakage scatter band and the horizontal line representing the fatigue limit of the matrix ϵ_m. This region corresponds to matrix cracking and interfacial shear failure. These two mechanisms are taken together in one band as they may occur simultaneously, particularly towards the end of fatigue life.

3.1.2 Stress ratio

Under constant amplitude loading conditions, strengths of composites depend on the magnitude of maximum and minimum stress states. In the literature, fatigue strengths are commonly studied as function of the stress ratio R expressed in terms of maximum stress σ_{max} and minimum stress σ_{min} by $R = \frac{\sigma_{min}}{\sigma_{max}}$. Fatigue strength of composite laminae such as glass and carbon fibre/epoxy depends on stress ratio [5,6] but changes little with load frequencies [5,7]. Under fatigue load conditions, there are different states of stress at different points in the material. Also after applying fatigue load, failure initiates near the stress concentrations and the material property degrades, therefore the stress ratio and the state of stress are not constant at each point [8]. In practice, stresses redistribute during the fatigue loading.

3.2 Fatigue of composites under elementary loads

Due to the degrees of complexity of composite structures, simplifications are made. The present approach tends to describe the structural behaviour in ply level: the so-called mesomodel [9]. Plies are considered to behave as an orthotropic material. The mechanical properties of plies are characterised under different elementary loading cases of a single type of ply:

- tensile and compressive load in fibre direction
- tensile and compressive load in transverse direction to fibres
- in-plane shear load
- interlaminar shear load

No coupling terms are considered here to define the structural behaviour for the case of bi-axial load.

The damage mechanisms of composites in fatigue environment are reviewed and discussed. The resulting failure of these damages depends on the type of reinforcement in the composite and whether the reinforcement is unidirectional or woven.

3.2.1 Fatigue damage of unidirectional composites under elementary loads

Degradation under load in fibre direction

The degradation of a UD-laminate subjected to longitudinal stress occurs typically through matrix microcracking perpendicular to the loading direction and fibre fracture [1].

Observations have shown that a high stiffness in the fibre presents a positive effect on residual strength under fatigue conditions. The use of very stiff fibres limits strain in the composite and thus in the matrix. This prevents large deformation

in the matrix which can lead to premature initiation of damage [10]. The SN-curve exhibits a more drastic drop in its fatigue strength when the composite is reinforced by low E-modulus fibres [1, 10]. GFRP is consequently more affected to cyclic loading in the fibre direction than CFRP.

The decrease of the residual stiffness is however more significant than the strength degradation [1]. Under tensile loading longitudinal to the fibre, a low loss of stiffness is observable for GFRP and CFRP [1, 5, 11]. Here matrix damage has a slight influence on the overall longitudinal stiffness of the composites especially when the fibre volume fraction is important [1,12]. Compressive fibre failure depends however mainly on fibre stability such as fibre micro-buckling and kinking.

Degradation under load transverse to fibres

The structural behaviour of composites under cyclic transverse loading is controlled by the mechanical properties of matrix and fibre-matrix interface [13]. The fatigue of polymers is characterised by initiation and growth of local cracks through the matrix and parallel to the fibres. As an isotropic material, rapid crack evolution arises from defects and asperity on surfaces until brutal failure [1].

Under cyclic load, the tensile and compressive parts of the stress do not contribute equally to the damage [5, 14]. For instance GFRP does not exhibit any reduction of the elastic modulus before the total failure of the laminate when subjected to compressive load [1] in contrast to a tensile loading.

Degradation under in-plane shear stress

UD composites under in-plane shear loading degrade principally through deterioration processes in matrix and in the interface between the matrix and fibres. Defects in the material depend highly on amplitudes of the cyclic shear loading. Small amplitudes in the order of 15-20% of the static strength bring on elastic deformation of the matrix, no matrix cracking is apparent [1]. Higher loading amplitude leads to matrix cracking in the interface between the matrix and fibres and parallel fibre breakage. This results in a rapid drop of the shear modulus over applied loading cycles [1].

Studies on $\pm 45°$-layers in carbon/epoxy shows that the drop in residual shear strength is low (drop up to 13% before failure) and may be neglected in a numerical model [11].

3.2.2 Fatigue damage of woven fabric composites

The structural behaviour of woven fabrics differs from UD composites particularly due to weave pattern and fibre volume fraction. They are particularly subjected

to matrix microcracking, fibre breakage, crack coupling and fibre-matrix interfacial debonding [10].

Fatigue damage of woven fabric layers

Similarly to UD laminates, a woven ply shows a brittle elastic behaviour when subjected to tension [15]. The damage occurring in these directions does not affect the behaviour of the ply under traction loading. Here the material is assumed to be brittle and non-sensitive to the cyclic loading in the direction of the fibres according to the authors.

Contrary to the behaviour of UD composites, woven fabric laminates show a high resistance to delamination and are not subjected to transverse rupture [16]. The application of in-plane shear loading also leads to a decrease in the shear modulus due to the generation of some fibre/matrix decohesions and matrix cracks [15].

Analogy with UD-layers

A numerical model is suggested which consists in replacing the woven plies by two stacked unidirectional plies corresponding to the warp and weft thicknesses [17]. Classical laminate theory is applied here and tends to describe the behaviour of the material by defining UD virtual plies with the same orientations than the warp and weft directions. These UD plies are considered separately for the analysis where the influence of the load amplitude is neglected in the transverse direction.

P. Curtis and B. Moore [18] compared the behaviour of laminated woven CFRP composites with that of equivalent non-woven CFRP laminates. Replacing just the $\pm 45°$-layers in (0,$\pm$45) UD lay-ups with woven fabric had little effect on static and fatigue behaviour in reversed axial cyclic loading. Based on the same study, the stacking sequences $[+45, -45, 0, 90]_s$ and $[0, 90, +45, -45]_s$ respectively provide similar S-N curves for woven and non-woven coupons [10]. The fatigue strength of laminates with $[0, 90]$ stacking sequences is however lower than one of a woven fabric composite [10, 19].

3.3 Failure criteria

Progressive damage models often employ a failure criterion along with degradation models. Different failure criteria have been proposed in the literature such as maximum stress criterion, Hashin's criterion and Puck's criterion.

3.3.1 Maximum stress theory

The maximum stress theory predicts failure when the stresses in the principal material axes exceed the corresponding material strength. In order to avoid failure it

has to be ensured that the stress limits are not exceeded

$$-R_{\parallel}^{c} < \sigma_{\parallel} < R_{\parallel}^{t} \tag{3.1}$$

$$-R_{\perp}^{c} < \sigma_{\perp} < R_{\perp}^{t} \tag{3.2}$$

$$|\tau_{\perp\parallel}| < R_{\perp\parallel} \tag{3.3}$$

As soon as one of the inequalities above is violated the material fails by a failure mode which is associated with the allowable stress. This failure criterion does not take any interaction of stress components into account and therefore certain loading conditions such as superposition of tensile and shear stresses, lead to non-conservative results.

3.3.2 Hashin's failure theory

One of the first failure criteria applied in fatigue which distinguished fibre-failure and matrix-failure mode was proposed by Hashin and Rotem [20]. They derived the fatigue failure criterion from their formulation under static loading, which is stated in fibre mode as:

$$\sigma_1 = R_{\parallel}^{t} \qquad \text{for } \sigma_1 \geq 0 \tag{3.4}$$

$$|\sigma_1| = R_{\parallel}^{c} \qquad \text{for } \sigma_1 < 0 \tag{3.5}$$

and for the 2D inter-fibre failure:

$$\left(\frac{\sigma_2}{R_{\perp}^{t}}\right)^2 + \left(\frac{\tau_{12}}{R_{\perp\parallel}}\right)^2 = 1 \qquad \text{for } \sigma_2 \geq 0 \tag{3.6}$$

$$\left(\frac{\sigma_2}{R_{\perp}^{c}}\right)^2 + \left(\frac{\tau_{12}}{R_{\perp\parallel}}\right)^2 = 1 \qquad \text{for } \sigma_2 < 0 \tag{3.7}$$

In case of inter-fibre failure Hashin and Rotem proposed an elliptic equation, which depends on the transverse stress σ_2 and on the in-plane stress τ_{12}.

3.3.3 Puck's failure theory for 2D failure analysis

Puck's criterion [21] is a physically based phenomenological model aiming to predict failure at layer level of unidirectionally fibre reinforced polymer composites. The failure hypotheses are developed based on experimental observations and lead to the conclusion that the material should be treated as brittle. The theory formulated by Puck considers three-dimensional failure mechanisms, and applies non-linear analysis to simulate progressive damage due to microdamage, matrix cracking and changes in fibre angle with increasing strains. The determination of failure is achieved by a fracture hypothesis based on strengths which are only expressed in terms of stress. The stress thresholds are defined from experimental observations of failure for different elementary stress states composed of strengths in fibre-parallel

and fibre-perpendicular tension and compression ($R^t_\parallel$, $R^c_\parallel$, $R^t_\perp$ and $R^c_\perp$) and in-plane and out-of-plane shear ($R_{\perp\parallel}$ and $R_{\perp\perp}$). The different strengths form the constraints to establish a fracture condition in the in-plane stress space (σ_1, σ_2, τ_{12}).

Puck defines physically-based fracture conditions based on two sub-surfaces which represent distinct failure types of a UD-lamina: fibre fracture (FF) under tension and compression and inter-fibre fracture (IFF).

Puck's fibre fracture criterion

Puck's theory defines the FF criterion by two stress limits for the tension and compression mode. In the model presented by Puck in 1969 [21], the failure condition is simply expressed by

$$f_{E\ FF} = \begin{cases} \frac{\sigma_1}{R^t_\parallel} \text{ for } \sigma_1 \geq 0 \\ \frac{\sigma_1}{-R^c_\parallel} \text{ for } \sigma_1 < 0 \end{cases} \tag{3.8}$$

$f_{E\ FF}$ represents the stress exposure for fibre failure while $R^t_\parallel$ and $R^c_\parallel$ correspond to the strengths in the fibre direction defined as positive values. Fibre fracture is predicted for any of the two values $f_{E\ FF} = 1$.

Puck's in-plane inter-fibre fracture criterion

Puck's criterion for inter-fibre fracture of UD composites is also physically based on hypotheses and mathematical formulations appropriate for brittle fracture in the ideas of Coulomb [22] and Mohr [23]. The main hypothesis formulated by Mohr is the consideration of stresses on the fracture plane decisive for fracture. In the 2D formulation of Puck's theory [24], the IFF criterion depends on the transverse stress σ_2 and the in-plane shear stress τ_{21} as seen in the fracture curve in Figure 3.2.

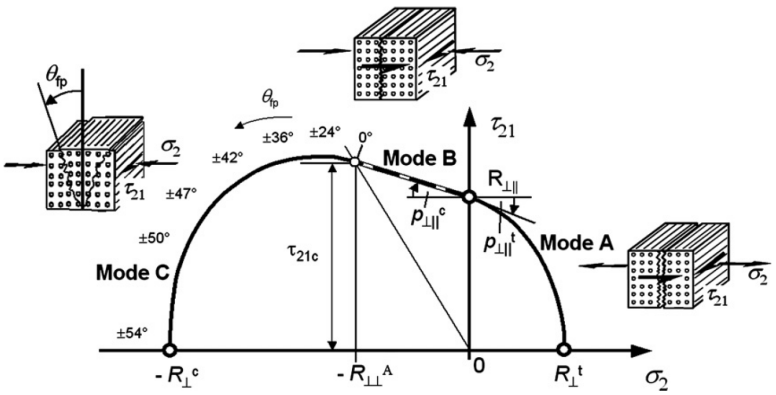

Figure 3.2: Predicted fracture curve from Puck's IFF criterion (from [25])

Three distinct cases are taken into account regarding IFF. The first one classified as mode A is caused by tensile stresses in the transverse direction and is described by Equation (3.9). When the stress exposure equals one, cracks are assumed to open transversely to fibres. The two other modes refer to failure under compressive stresses in the transverse direction. The IFF in mode B presented in Equation (3.10) initiates for relatively high values of in-plane shear and results in matrix cracking transversely to the normal stress direction. For a higher transverse compressive stress with respect to the shear stress such that $\left|\frac{\tau_{21}}{\sigma_2}\right| \leq \frac{|\tau_{21c}|}{R^A_{\perp\perp}}$, the failure is categorised in mode C and is expressed in Equation (3.11). This causes cracks in a plane that is not perpendicular to the one defined by the in-plane stresses. This refers to an catastrophic failure mode which could lead to delaminations and/or local buckling.

$$f_{E\ IFF}^{A} = \frac{1}{R_{\perp\parallel}} \left[\sqrt{\left(\frac{R_{\perp\parallel}}{R^t_{\perp}} - p^t_{\perp\parallel} \right)^2 \sigma_2^2 + \tau_{21}^2} + p^t_{\perp\parallel}\sigma_2 \right] \tag{3.9}$$

$$f_{E\ IFF}^{B} = \frac{1}{R_{\perp\parallel}} \left[\sqrt{\tau_{21}^2 + \left(p^c_{\perp\parallel}\sigma_2 \right)^2} + p^c_{\perp\parallel}\sigma_2 \right] \tag{3.10}$$

$$f_{E\ IFF}^{C} = \frac{\tau_{21}^2}{4(R_{\perp\parallel} + p^c_{\perp\parallel}R^A_{\perp\perp})^2} \frac{(-R^c_{\perp})}{\sigma_2} + \frac{\sigma_2}{(-R^c_{\perp})} \tag{3.11}$$

with $\tau_{21c} = R_{\perp\parallel}\sqrt{1 + 2p^c_{\perp\parallel}R_{\perp\perp A}/R_{\perp\parallel}}$, $p^t_{\perp\parallel}$ and $p^c_{\perp\parallel}$ are fitting factors which describe the strength in the transition zone from fibre-perpendicular stress to shear stress as depicted in Figure 3.2.

3.3.4 3D Puck's IFF theory

In the three-dimensional IFF criterion, the fracture condition is defined in the stress space (σ_1, σ_2, σ_3, τ_{12}, τ_{13}, τ_{23}).
The central consideration of Puck for IFF in 3D is the hypothesis that only three stresses act on a common action plane ($\sigma_\perp$,$\tau_{\perp\parallel}$ and $\tau_{\perp\perp}$) corresponding to three fracture resistances of the action plane R^A. The stress combination on any section plane of an isotropic material consists of one normal stress and one shear stress. In a UD lamina and as seen in Figure 3.3, the shear vector $\tau_{n\psi}$ can be expressed by means of two components acting on the action plane: τ_{nt} in transverse direction and τ_{n1} parallel to the fibre direction. A common stress action plane is then defined by only one normal stress σ_n and one resultant shear stress $\tau_{n\psi}$.

The action plane is inclined against the plane of σ_2 by the angle θ with the corresponding plane-related stresses. The consequence of the action plane-related fracture hypotheses is that in transversely isotropic materials there is an infinite number of action planes with potential fracture planes. The action plane corresponding with the highest risk of fracture should hence be identified from the stress components

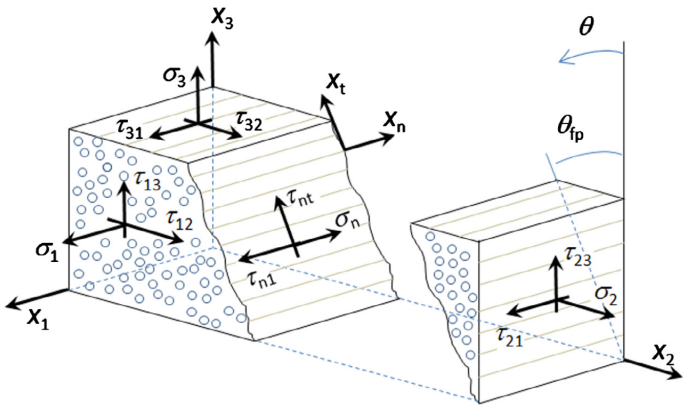

Figure 3.3: Fracture plane coordinate system (from [26])

and the fractures resistances. The criterion iteratively analyses the stress components on possible fracture planes perpendicular to the fibre direction and inclined by the angle θ to the axis of the thickness direction. This fracture angle corresponds to the angle θ_{fp} where stress exposure $f_{E\ IFF}$ in IFF is the highest. Stress exposure is expressed for fibre-perpendicular tension stress $\sigma_n \geq 0$ by Equation (3.12) and by Equation (3.13) for fibre-perpendicular compression stress $\sigma_n < 0$. IFF is predicted when the stress exposure reaches one.

$$f_{E\ IFF}(\theta) = \sqrt{\left[\left(\frac{1}{R_{\perp}^{At}} - \frac{p_{\perp\psi}^{t}}{R_{\perp\psi}^{A}}\right)\sigma_n(\theta)\right]^2 + \left(\frac{\tau_{nt}(\theta)}{R_{\perp\perp}^{A}}\right)^2 + \left(\frac{\tau_{n1}(\theta)}{R_{\perp\parallel}^{A}}\right)^2} + \frac{p_{\perp\psi}^{t}}{R_{\perp\psi}^{A}}\ \sigma_n(\theta) \tag{3.12}$$

$$f_{E\ IFF}(\theta) = \sqrt{\left(\frac{\tau_{nt}(\theta)}{R_{\perp\perp}^{A}}\right)^2 + \left(\frac{\tau_{n1}(\theta)}{R_{\perp\parallel}^{A}}\right)^2 + \left(\frac{p_{\perp\psi}^{c}}{R_{\perp\psi}^{A}}\sigma_n(\theta)\right)^2} + \frac{p_{\perp\psi}^{c}}{R_{\perp\psi}^{A}}\ \sigma_n(\theta) \tag{3.13}$$

3.4 Fatigue models

Various fatigue models are present in the literature and may be of very different nature. A short review of fatigue models is done with an emphasis on those which can be applied in the investigated application case.

3.4.1 Review of fatigue models

Fatigue modeling and life prediction may be classified into three main groups: fatigue life models, phenomenological models and progressive damage models [10, 27].

Fatigue life model

Fatigue life models do not account for any degradation mechanisms but use standard fatigue data such as S-N curves to predict fatigue failure. Most of the fatigue life models utilise a failure criterion as the base and an empirical fatigue curve as an input [10].

Philippidis and Vassilopoulos proposed a multiaxial fatigue failure criterion which is very similar to the Tsai-Wu quadratic failure criterion for static loading and produces acceptable failure loci [28]. The researchers preferred to use a multiaxial fatigue strength criterion based on the laminate properties, implying that for each laminate stacking sequence, a new set series of experiments is required [27].

El Kadi and Ellyin developed a model that is able to predict the S-N curve of a unidirectional laminate with arbitrary ply orientations and stress ratio [5]. A fatigue failure criterion for composite laminae based on input strain energy is proposed and requires a set of S-N curves to determine all the needed coefficients. The model is however sensitive to the choice of the reference S-N curve [27].

Phenomenological model to predict residual strength

Phenomenological models include a description of the damage in composites during fatigue loading where gradual deterioration of macro- and meso-mechanical properties is described through residual stiffness or strength models.

A phenomenological model based on residual strength uses experimental observation to describe the strength loss of composites and is subdivided into two models: sudden death model and wear-out model [10]. The residual strength in the sudden death model is kept constant over a certain number of cycles and is then suddenly degraded drastically when it reaches the critical number of cycles to failure N_f. This model is a suitable technique to describe this behaviour for high-strength unidirectional composites subjected to a high level state of stress [27]. The residual strength in the wear-out model is contrarily continually decreasing over the number of cycles following a certain predetermined equation. These models can be utilised at lower level states of stress. In the wear-out model according to Halpin et al [29], it is assumed that the residual strength $R(n)$ is a monotonically decreasing function of the number of cycles n, and that the change of the residual strength can be approximated by a power-law growth equation:

$$\frac{R^m(n) - \sigma^m}{R^m(0) - \sigma^m} = 1 - \frac{n}{N_f} \tag{3.14}$$

As reformulated by Shokrieh and Lessard [8] with m as a constant depending on the material. This model has been used by many authors in probabilistic and mechanistic models.

Extensive experimental investigation performed on glass/epoxy laminates showed no signs of degradation up to failure when it comes to residual strength under purely compressive fatigue or residual compressive strength under tensile fatigue [30].

Phenomenological model to predict residual stiffness

Residual stiffness models describe the degradation of the elastic properties during fatigue loading. To describe stiffness loss, the damage variable D is often used which is defined through the relation $D = 1 - E/E_0$, where E_0 is the undamaged modulus. The models are classified as phenomenological models and not as progressive damage models when the damage growth rate dD/dN is expressed in terms of macroscopically observable properties, and is not based on the actual damage mechanisms [27].

Several notable residual stiffness models have been developed and published technical publications [10, 27]. One of these models was presented by Whitworth [31]

$$E(n) = E(0)\left(\frac{S}{c_1 S_u}\right)^{\frac{1}{c_2}}\left[-h\ln(n+1) + \left(c_1\frac{S_u}{S}\right)^{\frac{m}{c_2}}\right]^{\frac{1}{m}} \tag{3.15}$$

where $E(0)$, $E(n)$, S_u and S respectively are initial stiffness, stiffness at n cycle, ultimate strength and applied stress. The parameters c_1, c_2, h and m are obtained from experiments.

Progressive damage model

Progressive damage models differ from the above mentioned models in the way that they are able to predict not only the number of cycles to failure but also local damage mechanisms via the use of fracture criteria. They are subdivided into two classes: damage growth models and models predicting residual mechanical properties.

Models predicting damage growth have been proposed to model damage accumulation for specific damage types such as matrix cracks and delamination. The evolution of transverse crack density and delamination size can for instance be used to describe the damage [10, 27].

Models predicting residual mechanical properties correlate the damage growth with the residual mechanical properties (stiffness and strength) to fully characterize the composite material. Shokrieh [8, 32–34] has constructed a model which is able to predict the fatigue damage progression of complicated composite structures. It requires however a full characterisation of the material based on the three loading of tension, compression and shear on fibres and resins by determining experimentally the residual stiffness and strength besides S-N curves for each of the load combination [10].

3.4.2 Failure mode based on constant life diagram

A great number of fatigue tests are generally required to establish the S-N relationships for given composite laminates over the whole range of stress ratios. The use of a constant fatigue life diagram (CFL) also called Goodman diagram proves to be an efficient method for evaluating the S-N relationships for any stress ratios on the basis of a limited number of fatigue tests [35]. This diagram represents constant life contours drawn in the plane of alternating stress $\sigma_a = \frac{\sigma_{max}-\sigma_{min}}{2}$ and mean stress $\sigma_m = \frac{\sigma_{max}+\sigma_{min}}{2}$ as seen in Figure 3.4. This approach allows the evaluation of fatigue life under constant amplitude loading at any stress ratio for the entire range of loading types which are compression-compression (C-C), tension-compression (T-C) and tension-tension (T-T)

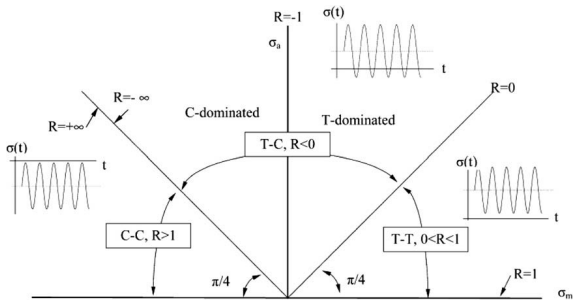

Figure 3.4: Annotation for $\sigma_m - \sigma_a$ plane [36]

CLD models

Vassilopoulos et al [36] examined the influence of the constant life diagram (CLD) formulation on the fatigue life prediction of composite laminates. They concluded that the selection of an accurate CLD formulation is essential for the overall accuracy of a fatigue life prediction methodology. Some choices of the CLD formulation can produce very conservative or very optimistic S-N curves which is directly reflected in the corresponding life assessment. They also showed that the relatively simple piecewise linear formulation proved to be the most accurate of the six compared formulations when a reasonable number of S-N curves (>3) is available. On the other hand, the diagram is distorted by the questionable assumption that all CLD lines converge to the UTS and UCS when R tends to one. [30]

CLD of on-axis and off-axis fatigue loading conditions

CLD diagrams for CFRP laminates often exhibit significant non-linearity [35]. The approach used by Kawai et al consists in evaluating the S-N relationships of composite laminates on a ply-by-ply basis. The CLD model is developed with a view to predict the fatigue behaviour of a UD composite ply under various modes of on-axis and off-axis fatigue loading conditions.

Kawai and Itoh [35] observed the sensitivity to mean stress in off-axis fatigue in the mode of fatigue loading i.e. tension-tension, tension-compression and compression-compression. Their study of the full shape of the off-axis CLD diagram for a UD carbon/epoxy laminate shows that the diagram becomes asymmetric about the alternating stress axis regardless of fibre orientation and correlates with the asymmetry in static strength in tension and compression. They came to the conclusion that the laminate exhibits highest sensitivity to off-axis fatigue, and thus degrades more significantly, under cyclic loading at the critical stress ratio, regardless of fibre direction.

3.4.3 Fatigue failure with Puck's criterion

In comparisons of many static failure theories against experimental data, the Tsai-Hill criterion was shown to be significantly non-conservative in predicting IFF in biaxial compression, whereas Puck's failure criterion was shown to be a good predictor of IFF under any loading condition [37–39].

Various methods have been developed to predict fatigue life based on a ply-by-ply approach using Puck's IFF criterion and a stiffness degradation model as well as a strength degradation model [7, 26, 30, 40]. In case of IFF modes A or B, which represent combined in-plane transverse tensile or compression and shear stresses, the stiffness degradation is modeled by various authors [26, 30, 40] according to Puck's model, and the stress is re-iterated with reduced stiffness parameters. IFF mode C, representing high transverse compressive and shear stresses, has to be regarded as critical with respect to the integrity of the laminate [26, 30, 40], as this mode is supposed to cause wedge shaped fracture fragments on a plane up to 51° [26, 40] leading to delaminations and local buckling [26, 30] and thereby precipitate failure of the laminate.

Kennedy et al [26] developed a stiffness degradation model depending on the IFF modes according to Puck. They consider that before IFF occurs, there is a significant fatigue degradation in the shear modulus for all IFF modes and a degradation of the transverse modulus only in compression (mode B and C). There is however little or no degradation of transverse modulus in mode A before IFF. In a type of failure corresponding to mode A, both the transverse normal modulus and the shear modulus of the lamina decrease sharply due to cracks. In contrast, after IFF in mode B the faces of the cracks do not separate as they are pressed together by the compressive normal stress leading to a softer decrease of the transverse modulus in comparison to that of mode A. The occurrence of IFF in mode C is assumed to lead to laminate failure and the numerical analysis is stopped.

Magin and Himmel [40] suggests to take into account material non-linearity and non-linear S-N curves to achieve a realistic estimation of the material behaviour under fatigue loading.

3.5 Macroscopic damage of composite lugs

Various macroscopic damage modes of composite lugs are described in this section and may be useful to characterise the failure modes of the tested specimens.

3.5.1 Shear fracture

Figure 3.5 illustrates a laminate which is detached from the bound in the loading direction through the entire lug thickness. The width of the detached strip corresponds to the diameter of the bolt. This mode of failure is principally encountered

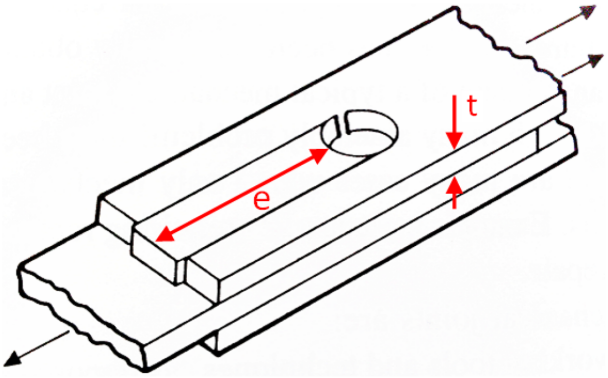

Figure 3.5: Shear fracture in composite lug (from [41])

when the hole of laminate is close to the front side [1]. This damage also occurs when the laminate contains few plies oriented at $\pm 45°$ to the loading direction. In the last case, the lug exhibits a shear stress concentration in the matrix at the edge of the hole. The shear strength of the whole laminate is therefore a decisive factor in the occurrence of lug failure. A rearrangement of the stacking sequence towards a laminate containing more $\pm 45°$ plies increases the shear strength of the structure.

3.5.2 Runaway behaviour of individual plies with same orientation

Similar to the shear fracture over the whole thickness of the lug, damage can occur by shearing in individual plies as depicted in Figure 3.6. In contrast to the previous failure case, a lower portion of the laminate thickness is affected by exhibiting detachments of isolated strips. As described previously, this damage mechanism typically arises when the lug is composed of many unidirectional plies gathered in blocks and oriented in the loading direction [1]. This stacking sequence causes an increase in the shear stress level. Off-axis plies remain firstly intact especially at a long distance from the hole. Laminates which contain thick layers of plies with the same orientation have a higher probability to fail in this manner. The transition region of two plies with different orientations is also subjected to higher interlaminar

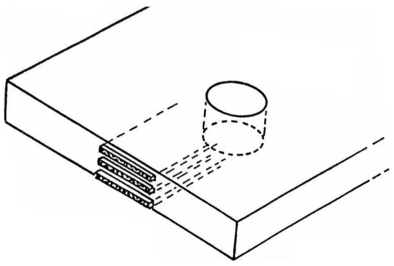

Figure 3.6: Runaway behaviour of individual plies with same orientation (from [42])

shear stress. A change of the ply orientation in the laminate allows to reduce these high magnitude of shear stress but increases also the manufacturing cost.

3.5.3 Combination of net section failure and dissociation

The combination of both one-sided flange fracture and dissociation is illustrated in Figure 3.7. Having a small portion of fibres in the loading direction favours

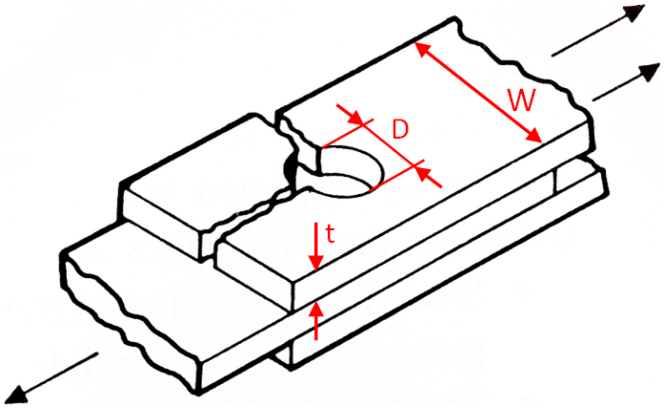

Figure 3.7: Combination of flange fracture and dissociation (from [41])

a cracking of the laminate [1] as depicted in the figure. Stress in this direction originates from transverse components which arises from the bolt by transmitting radial loading. Transverse stresses increase in the outer area of the hole. In order to reduce the probability of this failure, recommendations for avoiding shear failure as described previously should be applied. Inserting more 90° and ±45° plies has therefore a positive effect to avoid or delay the occurrence of such a failure.

Chapter 4

Progressive damage models

Based on different methods available in the literature and description of damage mechanisms, numerical models are proposed to predict the failure and damage of composite laminates under static and fatigue loading conditions. A model employing a Finite Element Method (FEM) is defined in Abaqus for numerical simulations of composite lugs and damage models are implemented in a user subroutine UMAT. The progressive damage model developed for the study in fatigue analysis is described in detail in the present chapter.

4.1 Modelling approach

The FEM model of the composite lugs analysed by experiments is established in Abaqus for both static and fatigue analyses. This model is specific to virtual testing of composite lugs with symmetric stacking sequences and subjected to an uni-axial loading in the longitudinal direction of the attachment.

4.1.1 Lug

The FEM simulation of the tensile test of the composite lug may be simplified in different ways. In the study, only the lug and a bolt in contact with the specimen are represented in the numerical simulation. The laminate of the lug has a symmetric stacking sequence and the specimen is considered to be subjected to a pure one-dimensional tensile load from the bolt in the longitudinal direction of the component. Three symmetric planes are therefore defined for the simulation as represented in Figure 4.1. Symmetry conditions are applied on the YZ plane located between the two holes of the lug, on the XZ plane cutting the parts through the thickness and the longitude and on the XY plane traversing the symmetry plane of the stacking sequence.

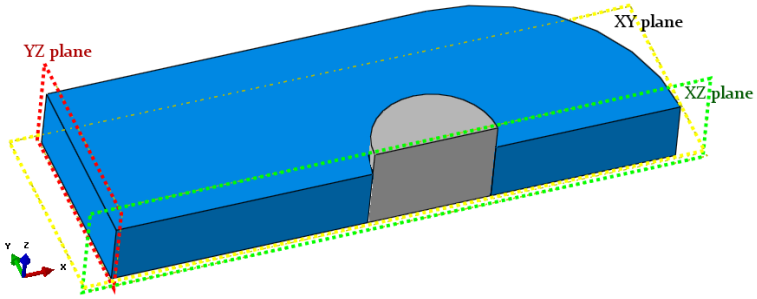

Figure 4.1: Symmetry conditions

4.1.2 Assembled model setup

The three-dimensional models of the lug and the bolt are meshed with brick elements as depicted in Figure 4.2. The region around the hole of the lug is refined since stress concentrations are expected at the vicinity of the hole. Different mesh refinements are used through the thickness with various attributions of the composite plies to brick elements for virtual testing in quasi-static analysis. Hard contact is applied

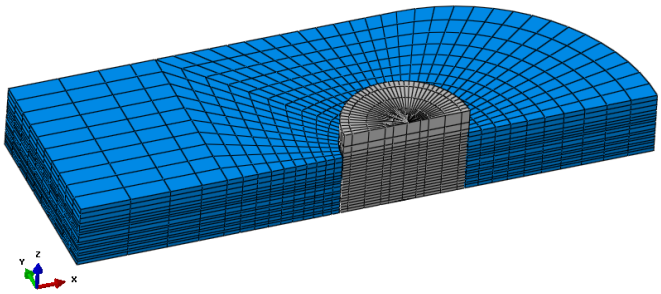

Figure 4.2: Visualisation of the mesh of the assembly

between the bolt and the hole's surface of the lug. The friction coefficient between the bolt and the laminate is not known. As part of a study on FEM-simulation of composite lugs, H. König [1] has performed a sensitivity analysis to investigate the influence of friction coefficients between a steel bush and the laminate in the predicted force at failure. The study showed that for various coefficients of friction in the range [0, 0.45], the resulting critical force may deviate up to 7%. In the present work, the friction's coefficient is estimated to be 0.2.

4.1.3 Bolt

When the lug is exposed to a tensile load, the reaction forces on the bolt induce a bending deformation of the bolt as seen in Figure 4.3. The bolt is hence considered elastic in the FEM simulation to gain in accuracy. A multi-point constraint (MPC)

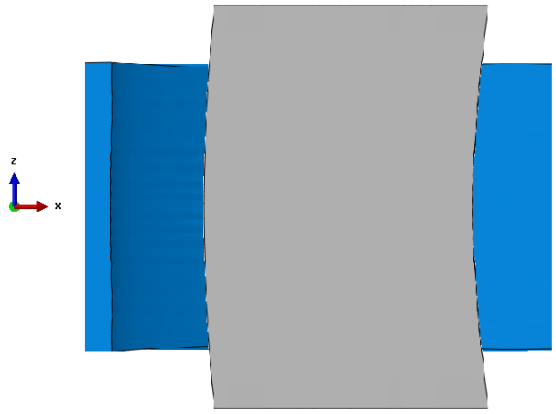

Figure 4.3: Deformation mode of the bolt

is used to connect the degrees of freedom of the upper surface of the bolt with a reference point set at the middle of the bolt (on the XY symmetry plane) as depicted in Figure 4.4. A displacement of this reference point is performed along the longitudinal axis to simulate the displacement control of the bolt. Along the symmetry conditions of the bolt on the XY and XZ planes, the MPC ensures the pulling motion of the bolt against the lug's hole.

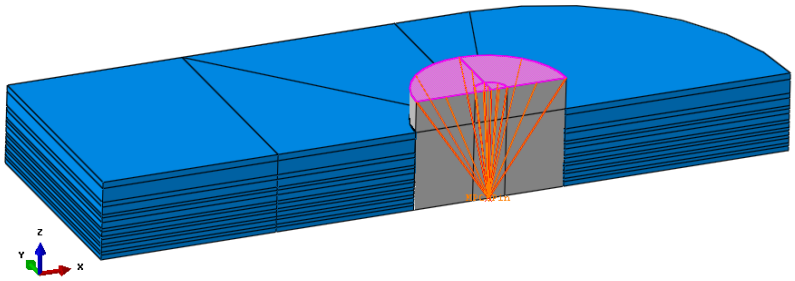

Figure 4.4: Representation of the multi-point constraint

4.2 Failure modelling

Stiffness degradation models at failure are presented for both quasi-static and fatigue analyses. They come into play when their respective failure criterion is fulfilled. Two damage models are presented for unidirectional plies along with Puck's theory: one for plane stress analysis and the other for three-dimensional stress analysis, and one stiffness degradation model for woven fabric plies. Finally a regularisation method is explained with a view to improve the convergence of the solutions.

4.2.1 2D damage model for a unidirectional ply

Associated with the fibre failure criterion (Equation (3.8)) and the 2D Puck's IFF criterion (Equations (3.9) to (3.11)), a damage model developed by Puck is used to degrade plane elastic properties. For this model, $E_{\parallel}$ refers to E_1, $E_{\perp}$ to E_2 and finally $G_{\perp\parallel}$ to G_{12}. The first version of the fatigue subroutine developed here uses the 2D damage model presented below. Out-of-plane stresses are considered not to participate in the material deterioration.

Fibre failure in compression and tension leads to catastrophic damage causing final failure due to the high energy release and its impact on the overall structural integrity of the laminate [30]. For this reason, a sudden degradation policy is used for fibre failure represented by a rapid drop of the stiffness as suggested by Kennedy et al [26]. The elastic modulus is hence abruptly degraded according to Equation (4.1).

$$E_{\parallel,f} = 0.1\ E_{\parallel} \tag{4.1}$$

For convergence reasons of FEA, the elastic modulus is not set to zero when fibre failure is predicted in a finite element.

For fibre dominated laminates under plane stress, IFF may not lead to a total loss of transverse and shear moduli of the failed ply in the vicinity of the occurring crack [30]. UD plies are confined inside a multidirectional lay-up which enables stress transfers from adjacent plies towards the failed one when moving further away from the damaged region. Cracked plies contribute consequently to the overall load bearing capacity of the laminate and the crack is observed macroscopically. Puck's model describes the degradation of $E_{\perp}$ and $G_{\perp\parallel}$ according to the following equation:

$$E_{\perp,f} = \eta_E\ E_{\perp,f(IFF)} \tag{4.2}$$

$$G_{\perp\parallel,f} = \eta_G\ G_{\perp\parallel,f(IFF)} \tag{4.3}$$

Here $E_{\perp,f}$ and $G_{\perp\parallel,f}$ are the degraded modules, $E_{\perp,f(IFF)}$ and $G_{\perp\parallel,f(IFF)}$ the secant-modules at IFF-initiation. The degradation factors η_E and η_G are defined according to the following equation:

$$\eta_E = \frac{1-\eta_{rE}}{1+c_E(f_{E\ IFF}-1)^{\xi_E}} + \eta_{rE} \tag{4.4}$$

$$\eta_G = \frac{1-\eta_{rG}}{1+c_G(f_{E\ IFF}-1)^{\xi_G}} + \eta_{rG} \tag{4.5}$$

c, ξ and η_r are parameters fitted on stiffness degradation data. Based on calibration from experimental data, Table 4.1 presents recommended values of these parameters for GFRP [43]. This stiffness degradation model is used by different authors to simulate fatigue damage considering in-plane stress state [26, 30]. The in-plane shear fatigue modulus is degraded following the mentioned method for IFF mode A and B. The loss in elastic modulus in transverse direction from Equations (4.4)

Parameter	$E_\perp$	$G_{\perp\parallel}$
c	5.3	0.70
ξ	1.3	1.5
η_r	0.03	0.25

Table 4.1: Recommended parameters for the degradation functions Equations (4.4) and (4.5) for GFRP

and (4.5) governs material deterioration in IFF mode A. IFF in mode C is considered as the most critical one as it is related to a high risk of delamination. A sudden degradation rule is applied at the occurrence of this type of failure similarly to fibre failure. The stiffness degradation model is summed up in Table 4.2.

Failure mode	Degradation imposed
FF	$E_{\parallel,f} = 0.1\ E_\parallel$
IFF mode A	$E_{\perp,f} = \eta_E\ E_{\perp,f(IFF)}$
	$G_{\perp\parallel,f} = \eta_G\ G_{\perp\parallel,f(IFF)}$
IFF mode B	$G_{\perp\parallel,f} = \eta_G\ G_{\perp\parallel,f(IFF)}$
IFF mode C	$E_{\perp,f} = 0.1\ E_\perp$
	$G_{\perp\parallel,f} = 0.1\ G_{\perp\parallel}$

Table 4.2: Degradation of elastic properties according to failure mode

4.2.2 3D damage model for unidirectional ply

A 3D degradation procedure presented by Deuschle [44] is used along with the three-dimensional Puck's criterion (Equations (3.8), (3.12) and (3.13)). The degradation process depends on the orientation of the IFF fracture plane which quantifies the amount of stiffness degradation. It tends to define the two fracture plane orientations which have the most direct (md) and least impact on the load bearing capacity of a lamina against the respective types of load. A coefficient $n(\theta_{fp})$ is then defined as expressed in Equation (4.6) to describe the fracture orientation-dependent impact of the degradation on the respective stiffness with values from $n_{min} \geq 0$ corresponding to the least impact to 1 for the most direct impact.

$$n = \left[\frac{1 - n_{min}}{2} \cos\left[2(\theta - \theta_{md}\right]\right] + \frac{1}{2} + \frac{1}{2} n_{min} \tag{4.6}$$

The recommended values of the most direct impact angle are summarised in Table 4.3. This orientation impact measure $n(\theta)$ weights the reduction of the respective

θ_{md}	E_2	E_3	G_{12}	G_{13}	G_{23}
n_i	0°	90°			
n_{ij}^+			0°	90°	+45°
n_{ij}^-			0°	90°	−45°

Table 4.3: θ_{md} controlling the impact of degradation on the respective stiffness depending on the fracture plane orientation θ_{fp} [44]

stiffnesses:

$$E_i^{red} = \begin{cases} E_i^{orig}(1 - n_i\ (1-\eta)) & \text{for tensile load in the } i\text{-direction} \\ E_i^{orig} & \text{for compressive load in the } i\text{-direction} \end{cases} \tag{4.7}$$

$$G_{ij}^{red} = \begin{cases} G_{ij}^{orig}(1 - n_{ij}^+\ k\ (1-\eta)) & \text{for positive } ij\text{-shear load} \\ G_{ij}^{orig}(1 - n_{ij}^-\ k\ (1-\eta)) & \text{for negative } ij\text{-shear load} \end{cases} \tag{4.8}$$

with k defined as the shear impact degradation measure and allows to reduce the shear stiffness less than transverse stiffness according to some suggestions from experimental observations [43, 45]. The recommended values are equivalent with the reduction of $G_{\perp\parallel}$ by only $k = 0.77$ for CFRC and $k = 0.41$ for GFRC of the reduction of $E_\perp$ [44].
η is the degradation progress measure which governs the degradation progress and can vary from one (no damage) to η_R (residual value). This plays a central role in the damage theory exposed by Deuschle. During the damage mechanism, it is supposed that the stress exposure is kept to unity as soon as IFF is reached. During the numerical analysis, if the stress exposure exceeds unity at a time increment, the value η is decreased and leads also to a decrease in the stiffness. This results in a decrease of the stress exposure through the diminution of stress magnitudes. Damage progress is therefore applied at each increment through an iterative process to fulfil the condition $f_{E\ IFF} = 1 = constant$ when damage occurs.

This 3D damage model is employed for UD plies in all simulations in quasi-static analysis and also in the latest damage model in fatigue analysis.

4.2.3 Damage model for woven fabric ply

Failure criteria and degradation models should be carefully selected for the analysis. Puck's criterion is in fact not appropriate for woven fabric layers. Applying this failure criterion would produce an underestimation of the transverse tensile strength because of the shape of the Master Fracture Body defined by Puck.

Another failure criterion should then be used for fabric layers. Two failure criteria are applied in the virtual testing of lugs: the maximum stress criterion and Hashin's criterion.

Regarding Hashin's failure criterion implemented in Abaqus, the material in the fabric layers is considered as brittle in the degradation model. Therefore, the material is considered to lose suddenly its stiffness at the occurrence of a failure.
The maximum stress criterion is applied for woven fabrics with a modified model of the 2D damage approach developed by Puck. It is assumed that the damage evolution in the wrap and weft directions of woven fabric plies is governed identically like unidirectional plies in fibre directions. When normal stress in wrap or weft direction reaches their respective strength $R_{\parallel}$ or $R_{\perp}$, a sudden stiffness degradation is applied. The maximum stress criterion is also applied for all shear stresses τ_{12}, τ_{23} and τ_{13} with the 2D damage model described in Equation (4.3) and in Equation (4.5).

4.2.4 Damage stabilisation

Material models exhibiting softening behaviour and sharp stiffness degradation typically show severe convergence difficulties in implicit numerical analysis. A local continuum damage model obeys the principle of local action. The problem with the local behaviour of a softening model is that as soon as a material point starts to soften, it takes up all the deformation [46]. Since all deformation occurs at the material point, damage only grows in that point, resulting in further softening. If damage models are included in the constitutive behaviour in a finite element analysis, then after localisation all the deformation accumulates in one element (or one row of elements). This makes the analysis mesh size dependent.

To improve the convergence rate of the iterative procedure without compromising the accuracy of the results [47] and to overcome the problem of mesh dependency in local damage models [46], a viscous stabilisation scheme is implemented as recommended by ABAQUS [48]. The procedure is a generalisation of the Duvaut-Lions regularisation model which expresses a stabilised damage variable as:

$$d^v = \frac{1}{\rho}\left(d - d^v\right) \tag{4.9}$$

ρ is the viscosity parameter controlling the rate at which the regularised damage variable d^v approaches the true damage variable d. However this stabilisation parameter should be properly selected and larger values can produce inaccurate results [47]. To update the regularised damage variable at time $t + \Delta t$, the equations are discretised in time as follows:

$$d^v|_{t+\Delta t} = \frac{\Delta t}{\rho + \Delta t}\, d|_{t+\Delta t} + \frac{\rho}{\rho + \Delta t}\, d^v|_t \tag{4.10}$$

The regularisation model of Duvaut-Lions is employed for the progressive damage models in quasi-static and in fatigue.

4.3 Progressive fatigue analysis

A progressive damage model is developed to predict failure of thick composite laminates. A ply-by-ply approach is used with a characterisation of the fatigue strengths for unidirectional and woven fabric plies at any stress ratio. Strength and stiffness degradation models are chosen to simulate damage progress of the laminate by the applied cyclic loading. Two models are proposed: the first version where only in-plane damage is taken into account and a second version considering three-dimensional degradation.

4.3.1 Ply characterisation

Fatigue strengths of a ply are described under cyclic loading in fibre direction, transverse direction and under shear loading to fully characterise the material for the model.

S-N curves of a UD ply

Fatigue strengths R_f are assumed to depend on the number of loading cycles to failure N_f and to be expressed in the form of

$$R_f = R_{end} + \frac{R_0 - R_{end}}{\exp\left(\frac{\log N_f}{\alpha}\right)^{\beta}} \tag{4.11}$$

R_0 is the static strength and R_{end}, α and β are curve fitting coefficients.

SN-curves associated to a UD laminate of E-glass/epoxy have been determined in fibre direction by a three point bending test for R-ratios in the tension-tension region (T-T) at 0.5, 0.2 and 0.05 and in the tension-compression (T-C) region at -0.5 and -1. A fatigue curve under ILS is also built from experimental tests at a R-ratio of -1.
Fatigue data in transverse direction is essential to establish a full model for the fatigue analysis. Further S-N curves under shear loading may also be needed to predict life in the "T-T" region more accurately. Due to a lack of experimental data regarding the present material of UD E-glass/epoxy composite, S-N curves for similar materials are employed. Passipoularidis et al. [30] determined S-N curves of a glass/epoxy UD composite for their model in fatigue life prediction. Definitions of the S-N curves under transverse and shear loading are displayed in Table 4.4. The formulation form of the S-N curve in Table 4.4 is a particular case of a general formulation of Equation (4.11) with $R_{end} = 0$, $\alpha = b/\ln(10)$ and $\beta = 1$.
The fatigue data in Table 4.4 is applied to characterise the material behaviour of the E-glass/epoxy UD composite in transverse direction and under shear loading for $R = 0.1$.

The present material E-glass/epoxy is stronger in transverse direction and under shear loading than the material used by Passipoularidis et al. From the comparison

Loading	R-ratio	S_0	b
Transverse	0.1	116.6	8.63
	-1	91.4	8.43
	10	196.8	24.32
Shear	0.1	83.8	11.16

Table 4.4: S-N curve [30]: $\sigma_{max} = S_0 N^{-\frac{1}{b}}$

of the static strengths between those different materials, it is assumed that our material E-glass/epoxy exhibits higher fatigue strengths in transverse directions than the material used as reference. S-N curves in transverse direction from the material used by Passipoularidis et al. are employed for the present model to define the fatigue behaviour of E-glass/epoxy in transverse direction to expect conservative results.

S-N curves for woven fabrics

The behaviour of woven fabrics is expected to differ from UD plies. Only S-N curve in interlaminar shear for $R = -1$ is available for woven fabric plies used in this study. Therefore several assumptions are made to establish a fatigue model in fibre directions and in in-plane shear for this material.

In a first model and similarly to the method used by Hochard et al. [17], woven fabric plies are replaced by two stacked unidirectional plies corresponding to the warp and weft thickness.

In a second model, the woven fabric plies conserve their elastic characteristics and static strengths. Assumptions are made on S-N curves and damage evolution models. Similar to the static analysis, the maximum stress criterion is applied for these woven fabric plies. The values of the static strengths are replaced by fatigue strengths from S-N curves. Hochard et al. [17] experimentally determined S-N curves of a woven fabric laminate in glass/epoxy. The composite is an unbalanced woven fabric laminate composed of 83% of the fibres running in the warp direction and 17% in the weft direction. The authors provided fatigue strengths corresponding to the wrap and the weft directions for the stress ratios $R = 0.1$ and $R = 0.5$. In the warp direction (0° ply laminates) only 5 fatigue strengths are reported whereas 18 values are displayed in the weft direction (90° ply laminates) for $R = 0.1$. For accuracy reasons, only S-N curves for the weft direction are exploited for the study. The values of the S-N curves were normalised by static strengths and the weft direction data is applied for both the wrap and weft directions in the presented model. The data is then adapted so that the S-N curves applied in the presented model includes the static strength at the origin of the graph. Figure 4.5 illustrates the S-N curves employed in our model for the wrap direction. The curve

for $R = 0.1$ is a curve fitted with the S-N curve model from the authors, and that of $R = 0.5$ is directly interpolated from experimental data for the associated stress ratio. The experimentally determined S-N curves under ILS loading for $R = -1$

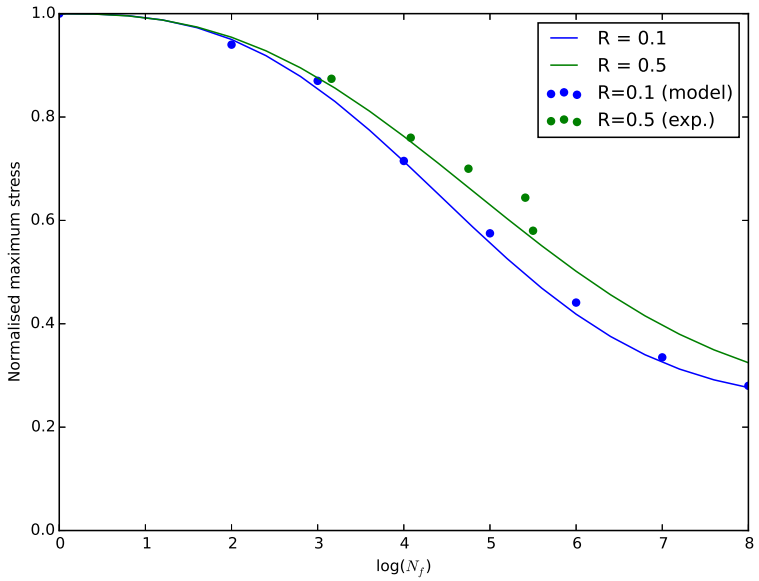

Figure 4.5: S-N curves in fibre direction for glass/epoxy woven fabric ply (adapted from [17])

are employed here for the wrap and weft directions. Regarding the in-plane shear behaviour of woven fabrics, S-N curves normalised by the static strengths of UD laminates are used to define the fatigue strengths.

Constant life diagram

The study aims to predict fatigue life under any stress ratio. A CLD method can hence be used in order to generate S-N curves at any loading conditions. A piecewise linear CLD is chosen due to its efficiency especially when S-N curves are available in more than three stress ratios [36]. Analytical expressions of the piecewise linear CLD can be described as follows [49]:

1. If R' is in the T-T sector of the CLD, and between UTS and the first known R-ratio in the tension region R_{1TT}

$$\sigma'_a = \frac{UTS}{\frac{UTS}{\sigma_{a,1TT}} + r' - r_{1TT}} \tag{4.12}$$

where σ'_a and $\sigma'_{a,1TT}$ are the stress amplitudes corresponding to R' and R_{1TT}, respectively, and $r_i = (1 + R_i)$, and $r' = (1 + R')/(1 - R')$.

2. If R is located between two known R-ratios, R_i and R_{i+1},

$$\sigma'_a = \frac{\sigma_{a,i}(r' - r_{i+1})}{(r_i - r')\frac{\sigma_{a,i}}{\sigma_{a,i+1}} + (r' - r_{i+1})} \tag{4.13}$$

3. If R' is in the C-C sector of the CLD, and between UCS and first-known R-ratio in the compression region R_{1CC}

$$\sigma'_a = \frac{UCS}{\frac{UCS}{\sigma_{a,1CC}} + r' - r_{1CC}} \tag{4.14}$$

where σ'_a and $\sigma'_{a,1CC}$ are the stress amplitudes corresponding to R' and R_{1CC}

A piecewise linear CLD is employed to generate S-N curves for any stress ratio in fibre direction, transverse direction and under shear loading. Figure 4.6 shows the CLD used for E-glass/epoxy UD plies in transverse direction.

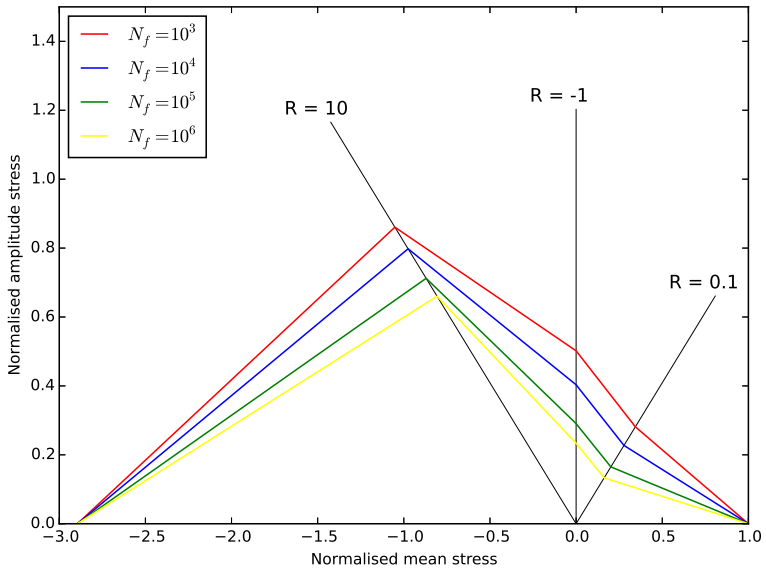

Figure 4.6: Piecewise linear CLD in transverse direction normalised by static tensile strength

Kawai et al. [35] have developed an asymmetric CLD partly based on a specific R-ratio χ designated as critical stress ratio which is defined as the ratio of the UCS to the UTS of the material. The authors assumed that the stress amplitude for

a given constant value of fatigue life is the greatest at the R-ratio χ [49]. This consideration is also taken in the present model in fibre direction of UD laminates, where linear interpolation of fatigue life in CLD is performed from the two regions separating the critical stress ratio line.

4.3.2 Strength degradation model

Fatigue damage accumulation is implemented in the algorithm based on residual strength degradation to be used along with a failure criterion. Residual tensile, compressive and shear strengths are considered while each residual strength component is treated as a function of loading cycles in their respective direction.

Residual strength after fatigue shows quite a large scatter, while a high experimental cost for material characterisation is required for implementing non-linear degradation models [30]. When tensile fatigue is considered for either glass/epoxy or carbon/epoxy laminates, the approach of a linear model proves to be the most efficient choice for describing residual degradation as it requires no residual strength tests and yields conservative predictions [50]. Life prediction methodologies show furthermore low sensitivity on the choice of the residual strength model [30].

The linear degradation model developed by Broutman and Sahu [51] is then considered for the tensile residual strength in the fibre direction $R^t_{\parallel f}$ as the following

$$R^t_{\parallel f} = R^t_{\parallel} - \left(R^t_{\parallel} - \sigma_{1\ max}\right)\left(\frac{n}{N_f}\right) \tag{4.15}$$

With σ_{max} the peak stress magnitude of the loading.

In a progressive damage model including stiffness degradation, stresses such as σ_{max} vary at points where damage occurs (loss in stiffness). This phenomenon happens also for the case of constant amplitude force due to stress redistribution from damage mechanism. Therefore a cumulative damage law may be interesting to improve the model. Adam et al. [52] described the fatigue response of a carbon-fibre composite through a wide range of experiments under variable amplitude loading. The authors concluded that in sequences of all-tension blocks of cyclic loading, a linear damage law (Miner's rule) was reasonably satisfactory, but in all-compression and mixed sequences the linear law drastically overestimates the actual composite life. However this rule does not permit the consideration of sequence effects, e.g. high-to-low or low-to-high stress amplitudes during a fatigue experiment [53]. Residual strength in fibre direction is then implemented as follows:

$$R^t_{\parallel f} = R^t_{\parallel} - \sum_{i=1}^{m}\left(R^t_{\parallel} - \sigma_{1\ max}\right)\left(\frac{\Delta n}{N_f}\right) \tag{4.16}$$

For the transverse tensile strength $R^t_{\perp f}$ and the in-plane shear strength $R_{\perp\parallel f}$ the model "Palmgren-Miner-rule" is applied directly as

$$R^t_{\perp f} = R^t_{\perp}\left(1 - \sum_{i=1}^{m}\frac{\Delta n}{N_f}\right) \tag{4.17}$$

$$R_{\perp\parallel f} = R_{\perp\parallel}\left(1 - \sum_{i=1}^{m}\frac{\Delta n}{N_f}\right) \tag{4.18}$$

As suggested by Magin [53] for the analysis of FRP structures, the damage variable is however limited to $\eta = 0.1$. The strength degradation models used under tension loading were also employed by Kennedy et al. [26] in their multi-axial fatigue damage model.

Under compressive cyclic loading, UD laminates do not display an evident strength degradation [1]. The linear strength degradation model of Broutman and Sahu can be modified to account for the sudden death behaviour of constant static strength up to fibre failure. The material non-linearity is introduced by inserting an exponent k having a high value to characterise the sudden death ($k > 20$ [30]) as expressed by Reifsnider [54]:

$$R^c_{\parallel f} = R^c_{\parallel} - \left(R^c_{\parallel} - \sigma_{max}\right)\left(\frac{n}{N_f}\right)^k \tag{4.19}$$

$$R^c_{\perp f} = R^c_{\perp} - \left(R^c_{\perp} - \sigma_{max}\right)\left(\frac{n}{N_f}\right)^k \tag{4.20}$$

4.3.3 Stiffness degradation model

Two phases of stiffness degradation are employed: one is applied prior to failure and another one when fibre failure or inter fibre failure occurs.

Pre-IFF stiffness degradation model

In general, all formulations of fatigue stiffness degradation agree on an initial drop of stiffness followed by a region of slow degradation with a steep fall immediately prior to failure. In the present context, a stiffness degradation rule as function of number of the loading cycles is implemented due to its simplicity. The non-linear residual stiffness model of Passipoularidis et al. [30] is implemented besides post-failure stiffness degradation models, with the following damage variable

$$\frac{E_{i,f}}{E_i} = 1 - (1 - \alpha_i)\left(\frac{n}{N_f}\right)^{\beta_i} \tag{4.21}$$

α and β are constant parameters fitted to stiffness measurements taken during fatigue testing. The values of the parameters for the glass/epoxy material employed

by Passipoularidis et al. are given in Table 4.5. Stiffness degradation as expressed in Equation (4.21) depends only on the fatigue life fraction while the stress level and R-ratio dependence are indirectly taken into account by the R-ratio dependent fatigue life N_f.

Parameter	$E_{\parallel}$	$E_{\perp}$	$G_{\perp\parallel}$
α	0.852	0.755	0.684
β	0.419	3.167	1.654

Table 4.5: Stiffness degradation property for UD glass/epoxy composite

The model is applied to reduce in-plane stiffnesses considering here that $E_{\parallel} = E_1$, $E_{\perp} = E_2$ and $G_{\perp\parallel} = G_{12}$ for unidirectional plies. The coefficients α and β in Table 4.5 relative to $E_{\parallel}$ are employed for woven fabric plies for both the wrap and the weft directions. This progressive damage is applied for all fatigue models before fibre failure and IFF.

Post-IFF stiffness degradation model

When failure occurs in unidirectional plies, the post-failure stiffness degradation models presented in Sections 4.2.1 to 4.2.3 are employed. For the 2D damage approach, the residual stiffness model in Section 4.2.1 is applied with the 2D fracture criterion in Equations (3.9) to (3.11) by replacing the values of static strength by residual strengths.

Similarly the three-dimensional failure criterion of Puck expressed in Equations (3.8), (3.12) and (3.13) are applied along with the 3D damage model of Deuschle in Section 4.2.2 for unidirectional plies. The equations defining the failure criteria are modified for fatigue degradation using the fatigue strengths of laminae instead of static strengths. Puck's IFF criterion in Equation (3.12) and Equation (3.13) become then

$$f_{E\ IFF}(\theta) = \sqrt{\left[\left(\frac{1}{R^{At}_{\perp}(N_f)} - \frac{p^t_{\perp\psi}}{R^A_{\perp\psi}(N_f)}\right)\sigma_n(\theta)\right]^2 + \left(\frac{\tau_{nt}(\theta)}{R^A_{\perp\perp}(N_f)}\right)^2 + \left(\frac{\tau_{n1}(\theta)}{R^A_{\perp\parallel}(N_f)}\right)^2} + \frac{p^t_{\perp\psi}}{R^A_{\perp\psi}(N_f)}\ \sigma_n(\theta) \tag{4.22}$$

for fibre-perpendicular tension stress $\sigma_n \geq 0$ and

$$f_{E\ IFF}(\theta) = \sqrt{\left(\frac{\tau_{nt}(\theta)}{R^A_{\perp\perp}(N_f)}\right)^2 + \left(\frac{\tau_{n1}(\theta)}{R^A_{\perp\parallel}(N_f)}\right)^2 + \left(\frac{p^c_{\perp\psi}}{R^A_{\perp\psi}(N_f)}\sigma_n(\theta)\right)^2} + \frac{p^c_{\perp\psi}}{R^A_{\perp\psi}(N_f)}\ \sigma_n(\theta) \tag{4.23}$$

for compressive normal stress $\sigma_n < 0$

4.3.4 Algorithm of the progressive fatigue damage

Fatigue analysis is performed by the FEA software Abaqus/Standard. First a quasi-static simulation is carried out in displacement control of the bolt until maximum reaction force is reached. It is followed by a fatigue analysis conducted without any motion of the bolt. During the analysis, blocks of cycles are applied at each time increment and stresses are calculated at integration points only for the case of an applied maximum force on the lug. Conway and Xiao [55] implemented a subroutine in Abaqus for their progressive damage model where a solution in fatigue was obtained for the maximum fatigue loading boundary condition and in turn, a solution for the minimum fatigue loading boundary condition was obtained by the specified stress ratio. In the presented model, only constant amplitudes and magnitudes of the applied force are considered with an attributed R-ratio $R_F = F_{min}/F_{max}$ in the range $[0, 1]$. The stress ratio is assigned for normal stresses as $R = R_F$ when the stress is positive and $R = 1/R_F$ when the stress is negative. The stress ratio in the case of a negative normal stress is therefore in the range $[1, \infty[$ corresponding to pure compressive cyclic loading. The stress ratio relative to shear stress is always equal to the stress ratio of the applied force due to the insensitivity of material properties regarding the sign of shear stress values.

Both fibre failure and IFF mode C are critical for the bearing capacity of the laminate due to the catastrophic behaviour of these damages. It is assumed that the structure fails as soon as one of this failure modes is encountered within a $0°$ ply or a $\pm 45°$ ply.

A user subroutine has been developed to be utilised by Abaqus in an implicit analysis at each time increment. The flowchart of the subroutine for the two-dimensional damage model is depicted in Figure 4.7 and the flowchart of the three-dimensional model is illustrated in Figure 4.8. Input variables from Abaqus are first read to recover from the values of residual stiffness, residual strengths and damage variables from the previous increment. The time increment provided by Abaqus is considered to calculate a fraction of life Δn that should be applied. From the strain increment, the stress tensor is calculated based on the residual stiffness matrix. In the next step stress exposures can be calculated by the application of a proper failure criterion (e.g. maximum stress or Puck's criterion). When failure occurs, the stiffness matrix

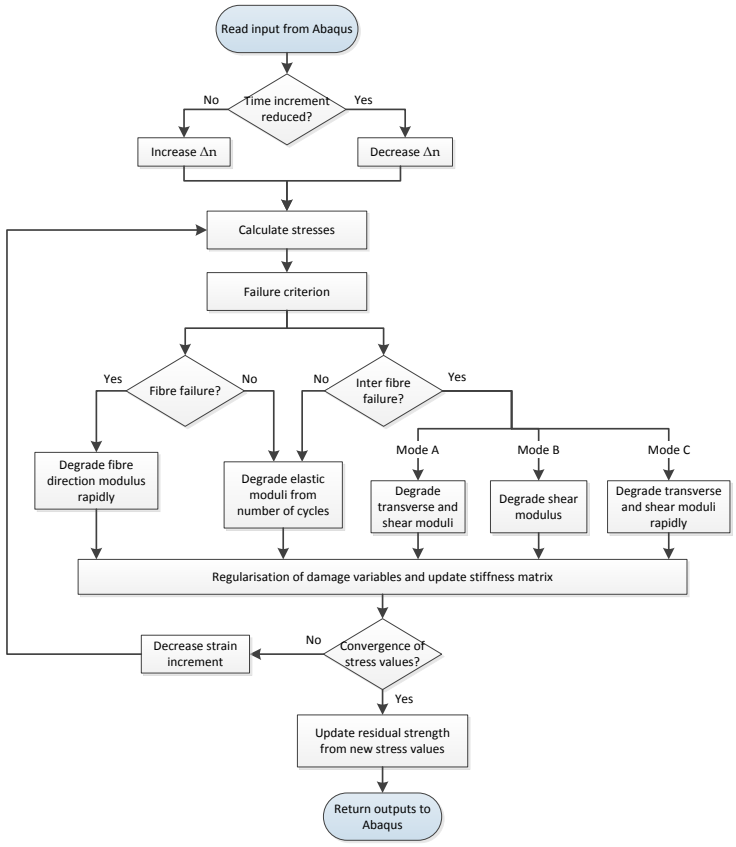

Figure 4.7: User subroutine flowchart for fatigue damage model in 2D

is degraded indirectly depending on the stress level by the failure criterion. The stress should then be recalculated by the new stiffness values which may lead to new damage states. Iterations are then required to have converged values of stress levels in order to harmonise variables with each other so that they change only to a very minor extent with each successive iteration [25]. In the case of the 3D damage model, iterations are also required to keep the IFF stress exposure constant to one when IFF occurs. Once stresses are finally calculated, the residual strength is updated by the use of S-N curves and the new stress state for the next increment. At an increment step, the residual strength is decreased if no damage occurs according to the strength degradation model.

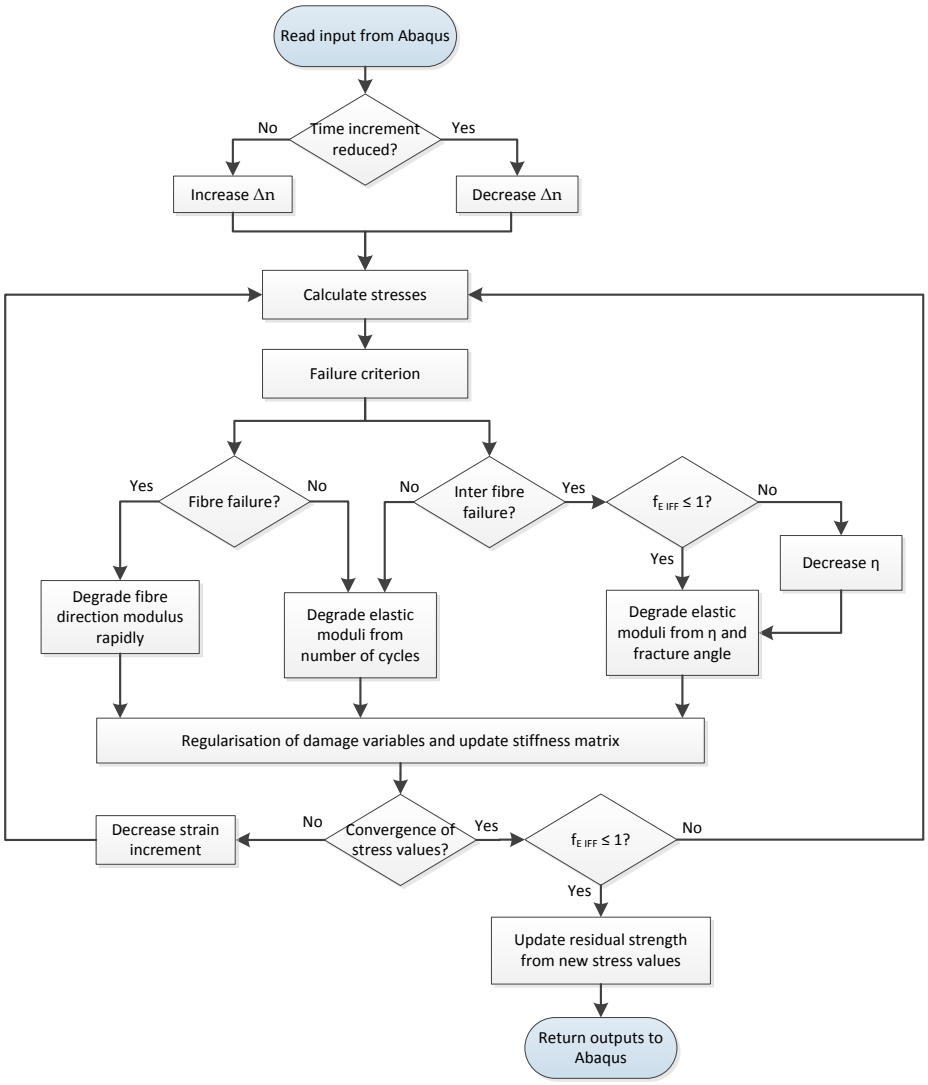

Figure 4.8: User subroutine flowchart for fatigue damage model in 3D

Chapter 5

Determination of failure and damage under static loading

Quasi-static simulations are performed on composite lugs using Puck's three-dimensional failure criterion and the damage model proposed by Deuschle with fracture angle dependency for unidirectional plies. Predictions of failure and macroscopic damage from virtual testing are then compared with experimental results.

5.1 Failure modes

The tensile loading of the bolt produces a stress concentration around the holes. As a consequence, the surface of the hole is the most critical zone for material degradation. Under increasing load, damage propagates towards the exterior edges of the lug.

The progressive damage of the composite lugs is studied here to understand the modes of failure of the laminates. The failure modes depend on the materials used as well as the stacking sequences. The progressive damage predicted from FEM is presented here for the specimens 1, 3 and 4.

5.1.1 Specimen 1

The failure of the specimen 1 is initiated by IFF of layers oriented at $\pm 45°$ and $90°$ due to transverse tensile stress. IFF occurs around the hole in the exterior surfaces of the component. The IFF of off-axis layers occurs from the outer surfaces to the inner surface due to the bending of the bolt which produces higher deformations in exterior plies. This deterioration evolves until all off-axis plies are damaged by IFF before any damage occurs in the off-axis layers.

Under increasing load, IFF of off-axis plies propagates to the exterior of the hole with a decrease of the stiffness in transverse direction to fibres. IFF in on-axis layers

initiates around in front of the hole. The damage in the 0° layers is caused by a combination of high in-plane shear stress and transverse tensile stress. It can be referred to IFF mode A according to Puck's theory. All on-axis plies are deteriorated in IFF before any fibre failure is expected.

First fibre failure is expected to occur in the outer +45° layers for all FEM models used (coarse and fine meshes through the thickness). This occurs around the hole in front due to tensile stress longitudinal to fibres. Under increasing load, FF occurs rapidly in other inner +45° plies. In a failure study of the same composite lug in numerical methods, König [1] also concluded that the specimen should first be damaged in 0° plies by shear failure. Matrix cracking is also expected to occur in the outer surface of the lug and to propagate in the different layers.

Figure 5.1 illustrates a comparison between a picture of a failed specimen 1 due to quasi-static loading and some results of the virtual testing. As shown in Figure 5.1a, the front section of the 0° layers is detached in longitudinal direction from the rest of the lug with a width corresponding to the diameter of the bolt. This corresponds to the runaway behaviour of individual plies with same orientation caused by a high shear stress as described in Section 3.5.2. It can also be noted that ±45° layers seem to be split around the yellow dashed line. At the state of first FF, the FEA models present regions where IFF occurred around the same section represented in a yellow dashed line in Figure 5.1b. The reduced in-plane shear stiffness of the 0° layers in front of the hole due to IFF may not be able to bear any increase of the load. This results in longitudinal crack in on-axis layers as seen in Figure 5.1a.

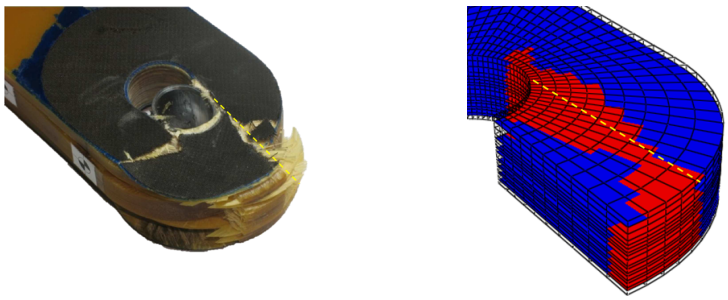

(a) Damaged specimen from quasi-static test

(b) IFF in red (reduced transverse stiffness)

Figure 5.1: IFF of specimen 1

Due to the fast propagation of FF within the +45° layers, the first fibre failure is considered to be critical regarding the bearing capacity of the lug.

5.1.2 Specimen 4

The progressive failure of specimen 4 is characterised by numerical simulation first by IFF of layers from the upper surfaces to the interior. IFF is observed within

on-axis UD layers, and off-axis fabric layers (±45° and 0°/90°) where all plies are damaged at the edge of the hole at a certain load step. Similarly to the failure mode of specimen 1, the 0° layers fail due to in-plane shear stress and the ±45° layers due to transverse stress.

After the propagation of IFF, fibre failure appears simultaneously in 0° and ±45° layers, where the number of affected layers rises rapidly with increasing load.

In the FEA simulation, on-axis UD layers made of glass-fibres are particularly affected by IFF with a damage region going from the hole to the front of the lug. The predicted IFF in 0° glass-fibre layers matches with the observed damaged layers. On-axis carbon-fibre UD laminae seem to be less affected to this type of failure. It

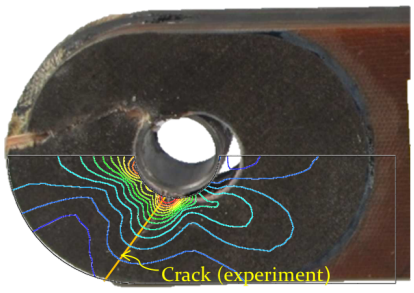

Figure 5.2: $f_{E\ IFF}$ contour shape in the upper ±45° fabric layers

can be noted that there is a good accordance of the type of failure of the lug's upper ±45° layers. By FE simulation, a crack orientation of 54° to the loading direction was expected to occur as shown in the gradient of the IFF factor in Figure 5.2. This result is consistent with the observed crack path from the experimental test and highlighted in the figure by the yellow solid line.

5.1.3 Specimen 3

Similarly to the previous case, specimen 3 is first damaged in the surface of the hole in IFF. At a certain load, all woven fabric layers are affected and IFF occurs in the UD layers at the exterior edges. With increase of the load, IFF propagates in all layers around the hole. Fibre failure appears after a further load increase in exterior ±45° plies and propagates with increasing load levels. At the end of the simulation all woven fabric layers are affected by FF around the hole.

5.2 Failure prediction

With the failure criterion discussed briefly in the previous section, results from the different numerical methods used are presented. Force-displacement diagrams are

plotted and failure conditions are discussed for the different specimens in comparison to the experimental data.

5.2.1 Specimen 1

Virtual testing has been performed under quasi-static loading conditions for different numerical models to evaluate their influence on the prediction of failure. Different FEM models have been used to predict total failure with a coarse mesh using one integration point through the thickness of the finite elements (1IP) and with three integration points (3IP). A refined model is also evaluated with a finer mesh within the laminate plane and the use of three integration points through the thickness.

As mentioned in the previous section, specimen 1 is supposed to fail soon after the occurrence of the first fibre failure in one ply. Figure 5.3 presents force-displacement diagrams for different numerical models where the values are normalised by the applied force at total failure of the experimental specimen which is also represented by the black dashed line at the unity.

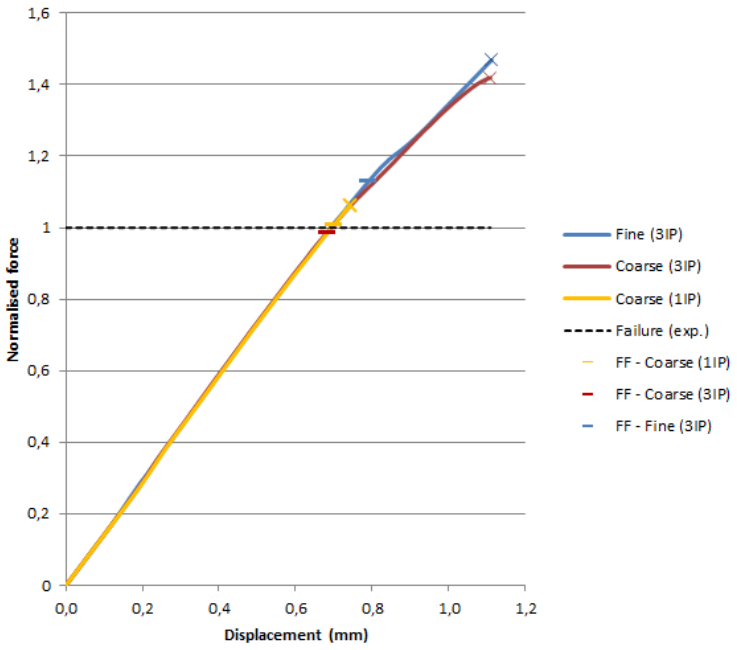

Figure 5.3: Force-displacement diagram for specimen 1

The corresponding values of first fibre failure are plotted by horizontal line markers and compared with the experimental value. Virtual simulations were stopped when the equilibrium was not any more ensured in non-linear analysis leading to a convergence issue of solutions (depicted by a cross marker). All FEM models predict a capacity of the lug to bear further increasing load after the first fibre failure up to

45% above the experimental value for the fine mesh FEM model.
The force at first FF given by the different methods are compared in Table 5.3 in normalised values with respect to the force at failure determined experimentally. The values at first FF show good agreement with that of total failure in the experiment. The choice of three integration points through thickness aids better convergence of the numerical model and only a slight discrepancy in the prediction of the first FF in comparison to the one integration point model. The shape of the force-displacement diagram of the fine model shows a significant difference when compared to the coarse mesh. The predicted value of the applied force at FF for the fine mesh is also 14.6% higher than one of the coarse mesh for the same number of integration points. This highlights the sensibility of the predicted failure loads on the choice of the through-thickness discretisation of the lug.

	Coarse mesh (1IP)	Coarse mesh (3IP)	Fine mesh (3IP)
Normalised force at last increment	1.06	1.42	1.47
Normalised force at first FF	1.01	0.99	1.13

Table 5.1: Applied force at failure of specimen 1

5.2.2 Specimen 4

The numerical models of specimen 4 combine different failure criteria as the lug consists of a mix of UD and woven fabric layers. Puck's criterion is employed for UD layers whereas the maximum stress criterion or Hashin's criterion are used for fabric layers. Three FEA models are tested here: a coarse mesh through the thickness with the use of the maximum stress criterion and Hashin's criterion for woven fabric layers and a fine mesh with the application of the maximum stress criterion. Failure is expected to occur soon after the occurrence of the first FF in on-axis UD layers. Force-displacement diagrams of the three approaches are plotted in Figure 5.4 as well as the applied force corresponding to the failure of the tested specimen. The force-displacement diagrams corresponding to the use of the maximum stress criterion with one and three integration points present some similarities here. They however predict a bearing capacity after the first FF in UD layers. In contrast, with the use of Hashin's criterion considering a totally brittle failure behaviour, total failure of the lug is predicted soon after the occurrence of first fibre failure by a rapid drop of the bearing capacity.

Table 5.2 compares the forces at first fibre failure with that from experiment. All virtual test results present reasonable predictions of failure considering that total failure is expected to occur at first FF. It can be seen that the use of Hashin's criterion as it is used for woven fabric layers leads to more conservative results than the application of the maximum stress criterion. The use of the maximum stress

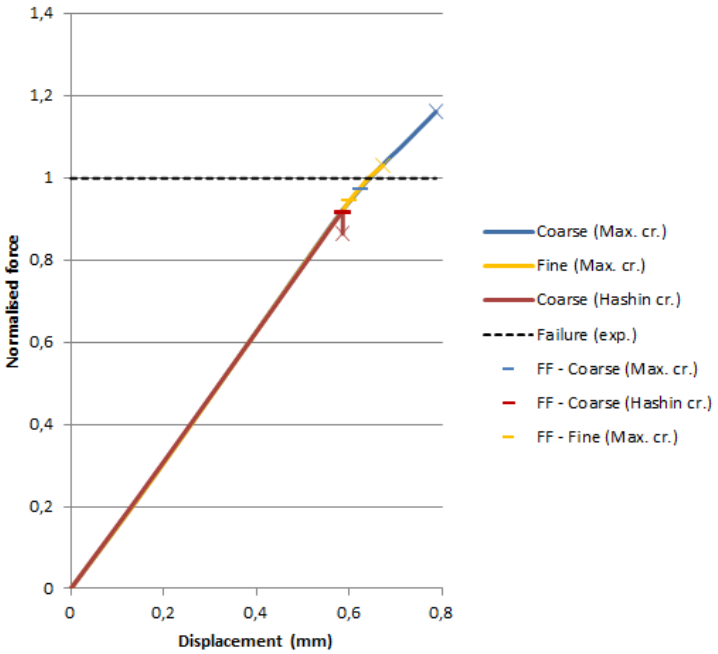

Figure 5.4: Force-displacement diagram for specimen 4

criterion and a coarse mesh provides the best results with an absolute relative difference of less than 3% in relation to the experimental value.

	Coarse mesh (max cr.)	Coarse mesh (Hashin's cr.)	Fine mesh (max. cr)
Normalised force at last increment	1.16	0.86	1.03
Normalised force at first FF	0.97	0.92	0.94

Table 5.2: Applied force at failure of specimen 4

5.2.3 Specimen 3

The virtual testing under quasi-static loading of the specimen 3 was performed with a coarse mesh in thickness direction of the lug. Since specimen 3 is also composed of fabric layers, the maximum stress criterion and Hashin's criterion were employed for the simulation of progressive failure. Experimental tests were conducted under three different conditions: one with flange bushings and two with bushings between the lug and the bolts. Failure was recorded with the use of flange bushings for the applied force $F_{exp.1}$ and at $F_{exp.2}$ respectively $F_{exp.3}$ for the two tests conducted with normal bushings. The best correlation between simulation and tests could be determined for the specimens with normal bushings. Therefore, the lowest first

failure load observed during the experimental tests with normal bushings is taken as reference for the FEA results.

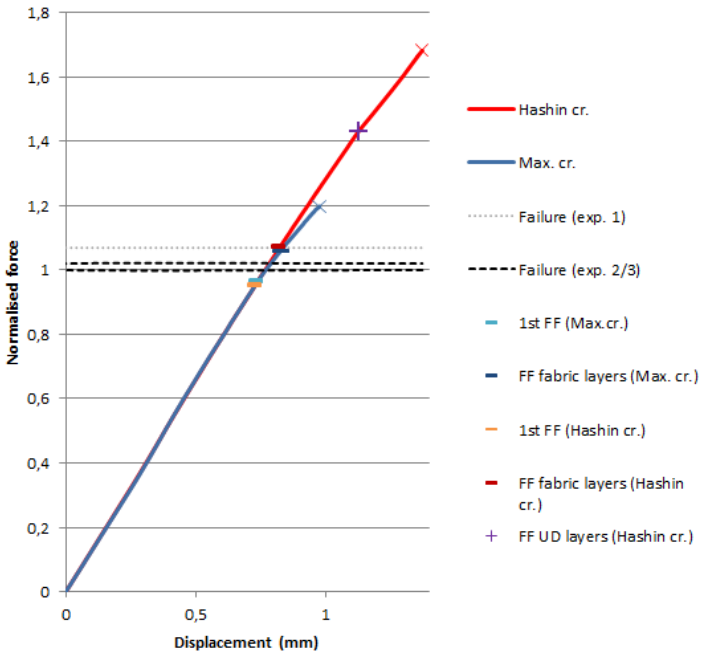

Figure 5.5: Force-displacement diagram for specimen 3

In Figure 5.5 the blue and orange line markers respectively refer to the force at first FF with the use of the maximum stress criterion and that of Hashin's criterion for woven fabric layers. In the same manner, the blue and red line markers refer to FF in all woven fabric layers when the maximum stress criterion or Hashin's criterion, respectively, is applied. The two values of force at total failure from test 2 and 3 are in the interval between the values of the predicted first FF and FF in all fabric layers for both failure criteria.

In this case the failure load predicted by Hashin's criterion are more conservative compared to the prediction by the maximum stress criterion as can be seen in Table 5.3. Considering that total failure of the lug occurs just after the first expected FF, both failure criteria deliver good predictions.

	Max. stress criterion	Hashin's criterion
Normalised force at first FF	0.96	0.95

Table 5.3: Applied force at failure of specimen 1

5.3 Discussion

The methods applied to estimate the force at failure of the laminate show good accordance with respect to the experimental results of the different specimens. The approach is based on the prediction of the total failure of a laminate once a fibre failure occurs in an unidirectional or $\pm 45°$ ply. The failure within a $\pm 45°$ ply is considered as critical for the lugs under investigation since this type of oriented ply represents a large portion of the laminate (more than one third in terms of volume) which may lead to a catastrophic drop of the bearing capacity of the lug. Nevertheless the simulations conducted foresee a relatively high bearing capacity far after the failure forces determined experimentally. The Puck's IFF model implemented for the unidirectional plies may underestimate the stiffness degradation within the laminate leading to discrepancies between FEA and experimental results.

Diverse finite element models and failure criteria for woven fabric layers have been tested and compared with the experimental results. The use of three integration points through the thickness of finite elements proved to improve the convergence of the solutions when compared to the choice of a single point. However the two alternatives do not show any discrepancy in the failure predictions. The failure predictions display a dependency on the mesh refinement in the stacking direction. A coarse mesh corresponding to the use of one element per block of identical plies produces better correlations in the failure prediction with experiments compared to the finer mesh. The benefit of a coarse mesh consists in applying a smeared damage approach which reduces the effects of local damage encountered in FEA. Moreover convergence issues have been detected with the fine mesh models resulting in the abortion of the simulations.

The application of the maximum stress criterion brings a better concordance with the experimental observations than the use of Hashin's criterion. The maximum stress criterion produces nonetheless non-conservative results as the coupling of different sorts of failure modes is not accounted for.

The previous highlighted results lead to the formulation of some recommendations for the failure predictions of composite lugs. The application of the total failure condition described above, the use of a relatively coarse mesh through the thickness of the laminate and the adoption of the maximum stress criterion within the woven fabrics prove to produce satisfactory predictions of the failure and damage of a lug subjected to an on-axis loading.

Chapter 6

Determination of failure and damage under cyclic loading

Once the progressive damage models are implemented, virtual tests on composite lugs are conducted to predict the fatigue life and the damage. Experimental tests have been conducted in order to measure the life of the composite specimens under cyclic loading at a constant amplitude. Since no S-N curve is available for the materials carbon/epoxy and R-glass/epoxy, the progressive damage models under fatigue loading conditions have been implemented only for pure E-glass/epoxy laminates. The experimental life predictions of hybrid laminates such as specimen 1 and 4 are then not exploited during this study. The present part focuses on the life prediction of the specimen 3 which is composed of unidirectional and woven fabrics in E-glass/epoxy. Based on the discussion in the previous chapter, the finite element model for the fatigue analysis is defined by a coarse mesh of the lug in the stacking direction consisting of 22 finite elements and by three integration points per element in the through-thickness direction.

An attempt of the life and damage prediction is made for the specimen 3 subjected to a fatigue loading condition which corresponds to a stress ratio $R = 0.14$.

6.1 Stress state at maximum force

In this section the stress state of the corresponding maximum force is described and discussed with a view to predict the fatigue life. In this analysis, the mechanical properties of the plies are assumed not to be deteriorated.

6.1.1 In-plane stress distribution

When loading the lug, stresses accumulate at the edge of the hole which may cause a damage initiation. According to this, the stress distribution of this surface is of great interest for the failure prediction and may require the construction of a new

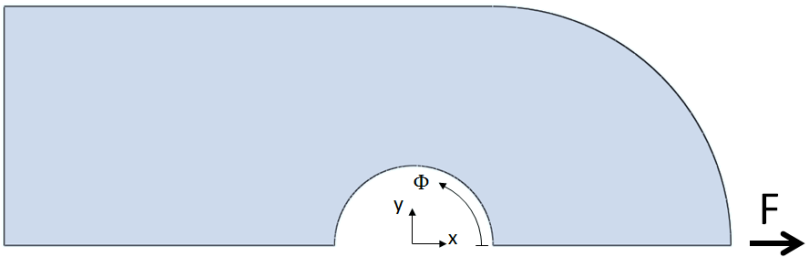

Figure 6.1: Global coordinate systems of the lug

frame of reference. Therefore a new cylindrical coordinate system is defined at the centre of the hole by the inclined angle ϕ from the x-axis evolving in the plane (x0y) as illustrated in Figure 6.1 and the through-thickness direction z. The layers which display the highest normal stress correspond to the 0° unidirectional plies. The bolt transmits loading into the front of the lug by compressive stress in the loading direction and mostly in the unidirectional plies. This produces high tensile stress in the UD plies at $\phi = 90°$ of the loading directional whereas shear stress remains rather low compared to that of off-axis woven fabric layers.

On the contrary ±45° woven fabrics carry most of the load by shear stress τ_{xy} at 45° to the loading direction. A large amount of this stress goes along the fibre directions of the off-axis woven fabric plies.

The first predictions in fibre failure can be expressed by analysing the level of stresses in fibre directions. This method does however not consider the influence of damage which can occur before total failure of the lug.

6.1.2 Fatigue life interpretation

The stresses at the corresponding maximum force are assessed in a linear analysis without any consideration of material deterioration. From the stress magnitudes and the S-N curves, it is possible to make some interpretations on possible damage and predicted life.

The stresses in fibre direction are of high interest since fibre fracture may cause a precipitate failure of the bearing component. The fracture criterion used in the presented model is furthermore simple as it only requires the stress in fibre direction and the fatigue strength data. The stresses in fibre directions are evaluated directly using the corresponding S-N curve regarding a possible fibre failure.

The maximum stress tensile and compressive values in fibre direction of UD plies are both considerably lower than the endurance limit of the S-N curve for the corresponding material and R-ratio. No fibre failure of the UD plies can hence be

predicted for this lug by a simple interpretation of the S-N curves.

Regarding the fabric layers, the maximum stress is reached at the hole's edge at $\phi = 45°$ from the loading direction in the $-45°$ outer ply. Figure 6.2 illustrates the two S-N curves employed for the investigated fatigue model at $R = 0.1$ and $R = 0.5$. The S-N curve in fibre direction for the stress ratio of the applied cyclic loading is hence interpolated from the two previous fatigue curves. The fatigue life corresponding to the maximum stress goes approximatively up to 6 290 000 loading cycles. The maximum compressive stress located in $+45°$ is far below the fatigue

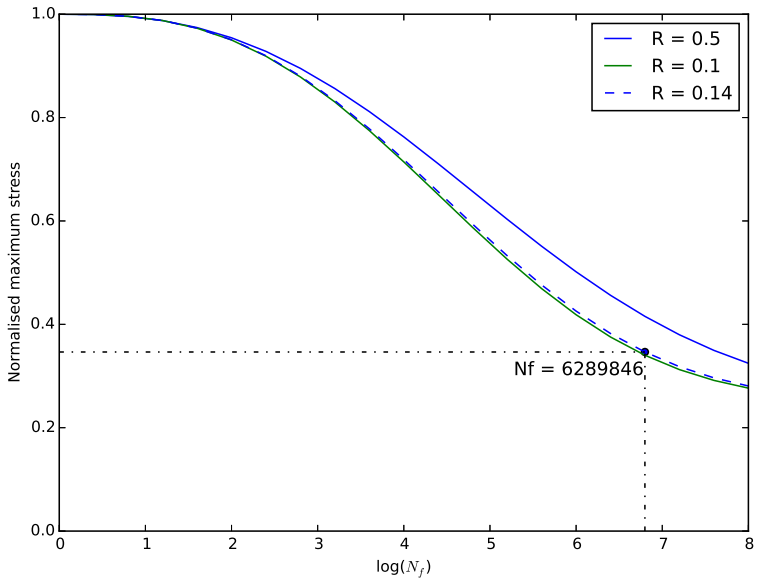

Figure 6.2: Life prediction under maximum tensile stress in fibre direction for $-45°$ woven fabric ply

limit.

6.1.3 3D stress state

One of the proposed progressive damage models is composed of a 2D failure criterion according to Puck's theory and its associated stiffness degradation model at inter fibre failure. This analysis neglects the effect of the three-dimensional stress state which arises from the loading transmission from the bolt to the tick laminate. The out-of-plane stresses are evaluated at the edge of the hole and discussed with respect to their respective strengths. Two stresses are considered to describe the 3D stress state: the normal stress in thickness direction $\sigma_3 = \sigma_z$ and the out-of-plane shear stress in the loading direction τ_{xz}.

The highest magnitude of the out-of-plane normal stress is located in the middle-plane of the laminate and approximatively at $\phi = 90°$ of the loading direction in the unidirectional layers. For the UD plies, it is assumed that the transverse and the through-thickness directions are characterised by the same S-N curves. Based on this assumption, the level of the highest out-of-plane normal stress is just below the fatigue limit of the material. Moreover the front of the hole exhibits out-of-plane compressive stresses reaching a maximum value in the middle of the laminate. This stress state takes its origin from the bending deformation of the bolt which causes a compression in the front of the lug. The compressive stresses encountered in the laminate are very low with respect to the high fatigue strength of the composite. In the two-dimensional model, it is assumed that compressive through-thickness stresses have a limited influence on the damage and the failure of the composite.

The highest out-of-pane shear stresses in the loading direction are located within the outer UD plies in the front of the hole. This shear stress concentration arises from the bolt which is in contact to the front of the hole and transmits in this manner some shear stress. Due to the bending deformation of the bolt, the shear stress reaches maximum values in the outer plies. The plies in the middle of the laminate exhibit quasi-null values of out-of-plane shear stress all around the hole. This corresponds indeed to the plane where a symmetry condition is applied. The highest value of shear stress is moreover far below the fatigue endurance for the corresponding S-N curve. The structure is therefore not expected to fail under this stress state when considered alone in the analysis and if the fatigue damage is assumed not to increase the stress level significantly.

The out-of-plane stresses remain low in comparison to their respective strengths. A high increase of the stress values under a cyclic loading is necessary to have an influence on the damage mechanism. However this out-of-plane stresses may interact with the transverse normal stresses σ_2 and the in-plane stresses σ_{12} leading to a complex damage state.

6.2 Damage prediction

An experimental test has been performed on the specimen 3 to determine the number of loading cycles when a failure occurs under a varying loading at the stress ratio $R = 0.14$. An attempt to predict the fatigue life with the developed progressive damage model is made. Two failure models and their associated damage methods are tested. The first damage model uses Puck's 2D failure criterion with an in-plane damage model. The second damage model is based on Puck's 3D failure theory with the associated 3D stiffness degradation law once the failure criterion is fulfilled. The two models use the same in-plane stiffness degradation model before failure.

6.2.1 Damage of the specimen

Pictures of the damaged lug are presented in Figure 6.3. Figure 6.3a shows a top

(a) Damaged specimen under fatigue loading conditions

(b) Lateral view of the runaway type of failure

Figure 6.3: Failure of the specimen 3 under fatigue loading condition

view of the specimen where damage is visible in the front of the right hole. The area presents some cracking on the outer surface crossing from the hole to the front at angles inclined to $\phi = 0°$ and $\phi = 45°$ of the loading direction. The lateral view of the damage shown in Figure 6.3b displays an apparent runaway failure of individual layers from the rest of the laminate. The dissociated plies observed in this figure correspond to woven fabric plies oriented at $\pm 45°$. All off-axis woven fabric layers seem to have failed in the front the hole. The rest of the laminate block represents on-axis unidirectional plies where no damage is clearly visible.

The observations of the specimen lead to the conclusion that failure of the lug occurs from failure of woven fabric plies.

6.2.2 Damage prediction by virtual testing

In the first finite element model, woven fabric layers are replaced by unidirectional layers oriented in the wrap and the weft directions. Multiple inter fibre failure is predicted in the corresponding woven fabrics by virtual testing on specimen 3 which lead to not negligible but also uncritical damage. Despite the drop of stiffness in shear and transverse directions, the lug is expected to be safe from fibre failure due to its high longitudinal strength. No failure of the laminate can then be predicted in the present fatigue loading condition.

In the second finite element model, fatigue behaviour of woven fabric plies is defined by existing S-N curves available in the literature and the maximum stress criterion is applied for the different degradation models. Progressive damage models implemented in 2D and 3D predict critical damage in unidirectional plies due to IFF. Failure of the lug is expected when first fibre failure occurs in $\pm 45°$ woven fabrics

whereas no damage in fibre directions is foreseen in UD plies.
The stiffness transverse to the loading direction is expected to decrease up to half of the initial stiffness along the entire front region of the hole. The damage region in woven fabrics are identical between the results from the 2D and 3D damage models. The first fibre fracture at ±45° ply occurs in the outer ply at an angle of $\phi = 45°$ with respect to the loading direction and determines failure of the lug. Fibre failures occur also sooner in 0°/90° woven fabrics in the hole and transverse to the loading direction. This failure is not considered to be critical in this specimen since 0°/90° woven fabric plies only represent a small portion of the laminate and there is still a high portion of 0° UD layers which can carry the load in that direction. According to virtual testing, the region affected by in-plane shear failure in woven fabrics does not propagate so far from the hole when compared to UD plies.

Figure 6.4 depicts residual properties at the failed point in ±45° ply for the critical direction (weft direction). As seen in Figure 6.4a, at the first phase of the life, the normal stress increases by 5% at approximatively 30 000 loading cycles. This can be explained by the stress redistribution from damaged to undamaged plies causing an increase of the load of undamaged layers. This phase is followed by a slight decrease in stiffness due to the damage process implemented in fibre directions before failure as shown in Figure 6.4b. This results in a decrease of the stress up to its initial value ($N_f = 0$) before failure. The residual strength decreases linearly with loading cycles and displays an exponential drop in the semi-logarithmic graph. Fibre failure occurs at 1 400 000 cycles when the stress in the fibre equals to the corresponding residual strength as indicated by the dashed line. After occurrence of fibre failure the stress drops due to the sudden stiffness degradation.

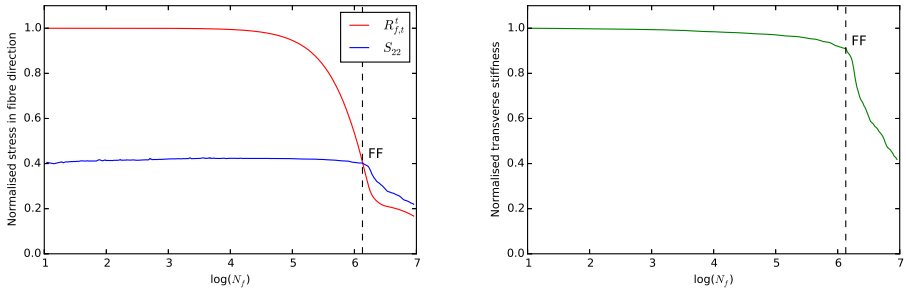

(a) Residual strength $R^t_{f,t}$ and stress S_{22} in weft direction

(b) Residual stiffness K_{2222} in weft direction

Figure 6.4: Normalised residual properties in 45° ply at the failed point

6.3 Failure prediction

Based on the discussion of the simulated damage state of the lug, the failure of the component is expected to occur at the first fibre failure in the ±45° woven fabric plies which happens for all the proposed models at the outer surface. The failure predictions are made based on three methods: the so-called linear model which does not take any damage into account and which corresponds to a direct interpretation of the S-N curves as explained in Section 6.1.2, the 2D progressive damage model and the 3D post-failure damage model.

The composite lug is predicted to fail after the application of $N_f = 6\ 300\ 000$ loading cycles according to the linear model, $N_f = 1\ 400\ 000$ cycles in the 2D model and $N_f = 2\ 100\ 000$ cycles in the 3D model. Under the same type of loading conditions, the specimen 3 failed after 480 000 loading cycles in the test. All the models provide here non-conservative predictions where the 2D damage model gives the best prediction accuracy with an error of factor 2.9.

Since all the S-N curves used to characterise the fatigue strength of the plies are formed in a semi-logarithmic scale, it is more pertinent to display strengths of the composite lug depending on the decimal logarithmic of the life. The force-life curves of the simulations are plotted in Figure 6.5 with normalised values with the static strength for the different numerical methods and with the experimental value. The fatigue curves are formed from simulations with the same stress ratio

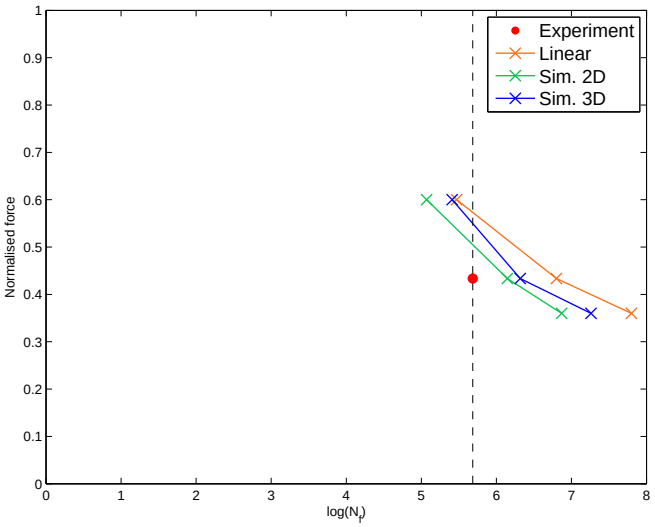

Figure 6.5: Fatigue strength of the composite lug

$R = 0.14$ for three different values of the maximum applied force: the force used in the experiment, one lower and one higher.

According to the two-dimensional damage model, the failure occurring at the life of the specimen corresponds to a normalised force of 0.5 instead of 0.43 when interpolating the fatigue life from the S-N curve. In order to have the same fatigue life, this corresponds to a relative error of maximum force at about 16% with respect to the applied force used in the experiment.

6.4 Discussion

An attempt of the life prediction of the specimen 3 under the fatigue loading condition at the stress ratio $R = 0.14$ has been made with the use of different methods. The life assessments show however some deviations when compared to the experimental result. This discrepancy can arise from different factors depending on the numerical approaches in the development of the fatigue models as well as the disposal of experimental results. The progressive damage models which have been implemented rely on many hypotheses regarding the fatigue strengths of the plies, the stiffness and strength degradation evolutions.

6.4.1 Reliability of the material behaviour

One of the main source of uncertainty in the different models which have been developed is the lack of data regarding the fatigue behaviour of the materials used in this study. The fatigue estimations which have been carried out on the specimen 3 tend to predict the failure of the lug at the first fibre failure of an off-axis woven fabric ply. In this application case, the fatigue predictions are then highly dependent on the stress-life diagram in the fibre directions of the woven fabrics as it determines the total failure condition of the laminate. Here the fatigue strengths in the wrap and weft directions of the E-glass/epoxy ply are assumed to be identical to a similar material of which fatigue data is available. This hypothesis has an influence on the accuracy of the so-called linear method and the progressive damage models.
The assumptions which have been made in the shape of the S-N curves of the unidirectional plies in the transverse direction and those of the woven fabric plies under in-plane loading may also have an indirect impact on the precision of the life assessment. In the presented progressive models, this set of data defines the initiation of stiffness degradation after failure. The simulated damage affects the critical ply by a stress distribution and has consequently an impact on the cumulative damage at the failed point. This may therefore accelerate or delay the total failure of the laminate.

The approach utilised in the investigated progressive damage models is globally conservative. The linear strength degradation models which have been applied under tensile loading are supposed to bring results on the conservative side [50]. The S-N curves of E-glass/epoxy plies in the transverse direction were also taken from those of a glass/epoxy material exhibiting a lower static strength in the respective direction. Therefore the predicted failure under the corresponding loading direction

is expected to occur prematurely. The stiffness degradation models applied during the simulations are also a significant source of uncertainty.

6.4.2 Approaches of the different fatigue models

No stiffness evolution has been experimentally determined under fatigue loading condition to validate the different models. Non-conservative damage evolution can however be expected for the use of the 3D fatigue model as observed in the nonlinear model under quasi-static conditions.

The linear model

The linear model employed does not take any damage into account until fibre failure. This method is not suitable for a high cycle fatigue analysis of such a complex application case. It however delivers a first estimation regarding the region subjected to failure as well as the fatigue life.

The progressive two-dimensional model

The stiffness degradation model employed in the investigated 2D model in IFF has been extensively used by various studies [26, 30, 40] along with Puck's failure criterion for plane stress analysis. The life assessment performed by these authors gives good agreement with the experimental results in the failure prediction of the laminates.

The lug is nonetheless subjected to a three-dimensional stress state due to the high thickness of the investigated laminate. The simulated out-of-plane stresses are relatively low when compared to their respective fatigue strengths (which are also estimated). They may nevertheless couple with the plane stresses leading to a complex fracture mechanism. According to Puck's theory, this affects the fracture angle of the failed plies which initiates a different damage mode.

An important factor which can affect the accuracy of solutions is the use of the regularisation method as expressed by Duvaut-Lions. The free-parameter ρ is indeed introduced in the stabilisation procedure and refers to a viscosity parameter which can control the rate of damage evolution. This variable may influence the solutions as observed in a study [56] which aims to predict the strength at a blunt notch within a laminate. The value assignment of the viscosity parameter can also be a source of deviation between the FEA results and the experimental results. A sensitivity analysis of the variable on the failure prediction may be required.

The progressive three-dimensional model

An attempt has been made to predict the fatigue life of a laminate with the use of the three-dimensional damage model expressed by Deuschle. The predicted life based

on this approach deviates more from the experimental value than the 2D damage model. The approach is based on the assumption that the equality $f_{E\ IFF} = 1$ should always be fulfilled during a damage process. In the simulations performed in fatigue, the stress exposure $f_{E\ IFF}$ often exceeds the unity which results in an underestimation of the stiffness drop in the failed points. This numerical issue is expected to delay the failure prediction by underestimating the increasing stress in the fibre directions due to the stress redistribution.

Decreasing the time increment may have a positive benefit to ensure that the stress exposure remains constant during a damage process. During a fatigue simulation, a great number of sudden drops of stiffness is encountered possibly due to the strength degradation process. The convergence can then be ensured by decreasing the time increment which, as a consequence, increases significantly the computational cost of the virtual test. The viscosity parameter applied in the damage stabilisation process plays also a role on the iterative process aiming to keep the stress exposure constant.

6.4.3 Validity of the models

In the present study, the models are tested along with only one experimental result which is not sufficient to evaluate the validity of the models. The failure under fatigue loading conditions has a more chaotic behaviour than under static loading inasmuch as high discrepancies can be observed in an experimental test of a laminate. Lives of specimens may vary up to a factor of 4 [7, 26, 30, 40] under the same fatigue loading conditions.

Furthermore sensitivity analysis may be required to test the robustness of the progressive damage models. This can be conducted by comparing solutions of a same virtual test with various mesh refinements and values for the damage stabilisation parameter ρ. The progressive damage models should also predict the fatigue life of laminates composed of different materials (hybrid laminate), subjected to diverse stress ratios and loading directions. Integrated to a rotor system, the lug receives also off-axis loading which has to be accounted for in a numerical simulation. Further virtual tests are therefore required to verify that the models can cover the failure predictions for any type of laminates and under different fatigue loading conditions.

Chapter 7

Conclusion

This work investigated the strength prediction of thick laminates under static and fatigue loading conditions. The focus was on the development of finite element models in order to conduct virtual testing of composite lugs subjected to an uni-axial loading. The presented numerical methods aim to become a tool for the design of thick composite lugs investigated by Airbus Helicopters but may also be used for any strength prediction of thick laminates. The laminates under study are composed of plies with various orientations, different types of reinforcement (unidirectional and woven fabric) and diverse materials (glass/epoxy and carbon/epoxy).

A review of the literature has been conducted on the damage and the failure of composite materials under fatigue loading conditions. The failure mechanism of composites subjected to uni-axial loading is described to characterise the fatigue behaviour of individual plies with the clear aim to apply the classical laminate theory. Based on the assessment of the different methods available in the literature, the development and the implementation of a progressive damage model has been chosen as it tends to predict the failure of any laminate and can also describe the damage evolution within the plies.

The failure prediction of laminates under quasi-static loading is carried out by a three-dimensional nonlinear model with the application of Puck's criterion for UD plies along with a damage model depending on predicted fracture angles and the use of the maximum stress criterion for woven fabrics. Two progressive damage models are developed for the fatigue analysis of laminates: one applies Puck's criterion for plane stress analysis with a 2D damage model and another one employs the failure criterion and the degradation model utilised for the quasi-static analysis. Based on the review of damage mechanisms and fatigue models, stiffness and strength degradation models are established and implemented in a user subroutine of the FEM software Abaqus/Standard.

Virtual testing on composite lugs is conducted under quasi-static loading for differ-

ent laminates and the predictions of the failure and the damage of the component are compared with the experimental data. Recommendations on the finite element model were drawn from the interpretation of the results regarding the mesh refinement and the number of integration points used in elements. The presented method proves to provide good predictions of failure and satisfactory results of the damage modes and may be used as a design tool.

The different investigated fatigue models are tested with an experiment on a composite lug. A plane stress analysis is made to establish a first life estimation of the component with respect to the fatigue strengths of the plies. The stress analysis also shows that the out-of-plane stresses are relatively low in the laminate which lead to a possible application of the investigated 2D damage model. The 2D damage model exhibits the best correlation with the experimental result in comparison to the 3D model but provides non-conservative results.

Further studies have to be conducted to validate and to improve the presented fatigue models. The main difficulties lie on the characterisation of the plies due to the lack of experimental data. Many assumptions have been made on fatigue strengths, stiffness and strength degradations relying on the data available in the literature for similar materials. Convergence issues have also been encountered in the application of the 3D damage model which may explain the underestimation of the damage and the failure of the component. The proposed numerical methods in fatigue analysis are not mature yet. However they highlight various aspects of the project where improvements or experimental data are needed in order to develop a reliable tool for the life prediction of thick composite lugs.

Bibliography

[1] H. König, "Untersuchung des Lochleibungsverhaltens dickwandiger Faserverbundlaminate unter kombinierter Zug- ung Biegebelastung," Master's thesis, Technische Universität Dresden, 2010.

[2] U. Butter, "Eurocopter Hubschrauber-Seminar 2004 Flugmechanik," 2004.

[3] O. Konur and F. L. Matthews, "Effect of the properties of the constituents on the fatigue performance of composites: a review," *Composites*, vol. 20, no. 4, pp. 317–328, 1989.

[4] R. Talreja, "Fatigue of composite materials: damage mechanisms and fatigue-life diagrams," *Royal Society of London*, vol. 378, no. 1775, 1981.

[5] H. E. Kadi and F. Ellyin, "Effect of stress ratio on the fatigue of unidirectional glass fibre/epoxy composite laminae," *Composites*, vol. 25, no. 10, pp. 917–924, 1994.

[6] N. Gathercole, H. Reiter, T. Adam, and B. Harris, "Life prediction for fatigue of T800/5245 carbon-fibre composites: I. Constant-amplitude loading," *International Journal of Fatigue*, vol. 16, no. 8, pp. 523–532, 1994.

[7] X. S. Sun, A. Haris, V. B. C. Tan, T. E. Tay, S. Narasimalu, and C. N. Della, "A multi-axial fatigue model for fiber-reinforced composite laminates based on Puck's criterion," *Journal of Composite Materials*, vol. 46, no. 4, pp. 449–469, 2011.

[8] M. M. Shokrieh and L. B. Lessard, "Multiaxial fatigue behaviour of unidirectional plies based on uniaxial fatigue experiments - I. Modeling," *International Journal of Fatigue*, vol. 19, no. 3, pp. 201–207, 1997.

[9] P. Ladevèze and G. Lubineau, "On a damage mesomodel for laminates: micro-meso relationships, possibilities and limits," *Composites Science and Technology*, vol. 61, no. 15, pp. 2149–2158, 2001.

[10] S. Wicaksono and G. B. Chai, "A review of advances in fatigue and life prediction of fiber-reinforced composites," *Journal of Materials: Design and Applications*, vol. 227, no. 3, pp. 179–195, 2012.

[11] J. Payan, *Etude du comportement de composites stratifiés sous chargement statique et de fatigue*. PhD thesis, Université Aix-Marseille II, 2004.

[12] G. Hartwig, R. Hubner, S. Knaak, and C. Pannkoket, "Fatigue behaviour of composites," *Cryogenics*, vol. 38, no. 1, pp. 75–78, 1997.

[13] B. D. Agarwal and L. J. Broutman, *Analysis and Performance of Fiber Composites*. John Wiley & Sons, 1990.

[14] M. S. Rosenfeld and S. L. Huang, "Fatigue characteristics of graphite/epoxy laminates under compressive loading," *Journal of Aircraft*, vol. 15, no. 5, pp. 264–268, 1978.

[15] C. Hochard, J. Payan, and C. Bordreuil, "A progressive first ply failure model for woven ply CFRP laminates under static and fatigue loads," *International Journal of Fatigue*, vol. 28, pp. 1270–1276, 2006.

[16] C. Hochard, P.-A. Aubourg, and J.-P. Charles, "Modelling of the mechanical behaviour of woven-fabric CFRP laminates up to failure," *Composites Science and Technology*, vol. 61, no. 2, pp. 221–230, 2201.

[17] C. Hochard and Y. Thollon, "A generalized damage model for woven ply laminates under static and fatigue loading conditions," *International Journal of Fatigue*, vol. 32, pp. 158–165, 2010.

[18] P. T. Curtis and B. B. Moore, "A comparison of the fatigue performance of woven and non-woven CFRP laminates in reversed axial loading," *International Journal of Fatigue*, vol. 9, no. 2, pp. 67–78, 1987.

[19] K. Schulte and C. Baron, "Schädigungsentwicklung bei Ermüdung verschiedener CFK-Laminate," *Zeitschrift für Werkstofftechnik*, vol. 18, pp. 103–110, 1987.

[20] Z. Hashin and A. Rotem, "A fatigue criterion for fibre reinforced composite materials," *Journal of Composite Materials*, vol. 7, no. 4, pp. 448–464, 1973.

[21] A. Puck and W. Schneider, "On failure mechanisms and failure criteria of filament-wound glass-fibre/resin composites," *Plastics & Polymers*, vol. 37, pp. 33–44, 1969.

[22] C. A. Coulomb, "Sur une application des règles de maximis et minimis à quelques problèmes de statique relatives à l'architecture," *Mémoires de Mathématique et de Physique*, 1776.

[23] O. Mohr, "Welche Umstände bedingen die Elastizitätsgrenze und den Bruch eines Materials," *Zeitschrift des VDI*, vol. 24, no. 45/46, pp. 1524–1541 & 1572–1577, 1900.

[24] A. Puck and H. Schürmann, "Failure analysis of FRP laminates by means of physically based phenomenological models," *Composites Science and Technology*, vol. 62, no. 12/13, pp. 1633–1662, 2002.

[25] A. Puck and M. Mannigel, "Physically based non-linear stress-strain relations for the inter-fibre fracture analysis of FRP laminates," *Composites Sciences and Technology*, vol. 67, no. 9, pp. 1955–1964, 2007.

[26] C. R. Kennedy, C. M. . Brádaigh, and S. B. Leen, "A multiaxial fatigue damage model for fibre reinforced polymer composites," *Composite Structures*, vol. 106, pp. 201–210, 2013.

[27] J. Degrieck and W. V. Paepegem, "Fatigue damage modeling of fibre-reinforced composite materials: Review," *American Society of Mechanical Engineers*, vol. 54, no. 4, pp. 279–300, 2001.

[28] T. P. Philippidis and A. P. Vassilopoulos, "Fatigue strength prediction under multiaxial stress," *Journal of Composite Materials*, vol. 33, no. 17, pp. 1578–1599, 1999.

[29] J. C. Halpin, K. L. Jerina, and T. A. Johnson, "Characterization of composites for the purpose of reliability evaluation," tech. rep., American Society for Testing and Materials, Philadelphia, 1973.

[30] V. A. Passipoularidis, T. P. Philippidis, and P. Brondsted, "Fatigue life prediction in composites using progressive damage modeling under block and spectrum loading," *International Journal of Fatigue*, vol. 33, pp. 132–144, 2011.

[31] H. A. Whitworth, "A stiffness degradation model for composite laminates under fatigue loading," *Composite Structures*, vol. 40, no. 2, pp. 95–101, 1998.

[32] M. M. Shokrieh and L. B. Lessard, "Multiaxial fatigue behaviour of unidirectional plies based on uniaxial fatigue experiments - II. Experimental evaluation," *International Journal of Fatigue*, vol. 19, no. 3, pp. 209–217, 1997.

[33] M. M. Shokrieh, "Progressive fatigue damage modeling of composite materials - Part I. Modeling," *Journal of Composite Materials*, vol. 34, no. 13, pp. 1056–1080, 2000.

[34] M. M. Shokrieh, "Progressive fatigue damage modeling of composite materials - Part II. Material characterization and model verification," *Journal of Composite Materials*, vol. 34, no. 13, pp. 1081–1116, 2000.

[35] M. Kawai and N. Itoh, "A failure-mode based anisomorphic constant life diagram for a unidirectional carbon/epoxy laminate under off-axis fatigue loading at room temperature," *Journal of composite materials*, vol. 48, no. 5, pp. 571–592, 2013.

[36] A. P. Vassilopoulos, B. D. Manshadi, and T. Keller, "Influence of the constant life diagram formulation on the fatigue life prediction of composite materials," *International Journal of Fatigue*, vol. 32, no. 4, pp. 659–669, 2009.

[37] M. Hinton, A. Kaddour, and P. Soden, "A comparison of the predictive capabilities of current failure theories for composite laminates, judged against experimental evidence," *Composites Science and Technology*, vol. 62, no. 12-13, pp. 1725–1797, 2002.

[38] P. D. Soden, A. S. Kaddour, and M. J. Hinton, "Recommendations for designers and researchers resulting from the world-wide failure exercise," *Composites Science and Technology*, vol. 64, pp. 589–604, 2003.

[39] A. S. Kaddour and M. J. Hinton, "Maturity of 3D failure criteria for fibre-reinforced composites: Comparison between theories and experiments: Part B of WWFE-II," *Journal of Composite Materials*, vol. 47, no. 6-7, pp. 925–966, 2013.

[40] M. Magin and N. Himmel, "Physical non-linear of unidirectional polymer matrix composites in cyclic fatigue life analysis," 17th International Conference on Composite Materials, ICCM-17, University of Kaiserslautern, Edinburgh, Scotland, 2009.

[41] M. C. Y. Niu, *Composite Airframe Structures.* Hong Kong Conmilit Press Ltd, first ed., 1992.

[42] L. J. Hart-Smith, "Design and analysis of bolted and riveted joints in fibrous composite structures." Presentation, Long Beach, 1983.

[43] M. Knops and C. Bögle, "Gradual failure in fibre/polymer laminates," *Composites Science and Technology*, vol. 66, no. 5, pp. 616–625, 2006.

[44] H. M. Deuschle, *3D Failure Analysis of UD Fibre Reinforced Composites: Puck's Theory within FEA*. PhD thesis, Universität Stuttgart, 2010.

[45] M. Knops, *Gradual failure process in fibre/polymer laminates.* PhD thesis, RWTH Aachen, Institute für Kunststoffverarbeitung (IKV), 2003.

[46] M. S. Niazi, H. H. Wisselink, and T. Meinders, "Viscoplastic regularization of local damage models: revisited," *Computational Mechanics*, vol. 51, no. 2, pp. 203–216, 2012.

[47] C. G. Dávila, P. P. Camanho, and A. Turon, "Effective simulation of delamination in aeronautical structures using shells and cohesive elements," *Journal of Aircraft*, vol. 45, no. 2, pp. 663–672, 2008.

[48] ABAQUS 6.6 User's Manual, ABAQUS, Inc., Providence, RI, 2006.

[49] T. Park, M. Kim, B. Jang, J. Lee, and J. Park, "A nonlinear constant life model for the fatigue life prediction of composite structures," *Advanced Composite Materials*, vol. 23, no. 4, pp. 337–350, 2014.

[50] T. P. Philippidis and V. A. Passipoularidis, "Residual strength after fatigue in composites: Theory vs. experiment," *International Journal of Fatigue*, vol. 29, no. 12, pp. 2104–2116, 2007.

[51] L. J. Broutman and S. Sahu, "A new theory to predict cumulative fatigue damage in fiberglass reinforced plastics," *Composite materials: testing and design (2nd Conference), ASTM STP 497*, pp. 170–188, 1972.

[52] T. Adam, N. Gathercole, H. Reiter, and B. Harris, "Life prediction for fatigue of T800/5245 carbon-fibre composites: II. Variable-amplitude loading," *International Journal of Fatigue*, vol. 16, no. 8, pp. 533–547, 1994.

[53] M. Magin, *Innovative Design, Analysis and Development Practices in Aerospace and Automotive Engineering*, ch. Recent Developments of Mechanical and Fatigue Analyses of Fiber-Reinforced Structures for Aerospace Applications. Springer, 2014.

[54] K. L. Reifsnider, *Fatigue of Composite Materials*, ch. Damage and damage mechanics. Elsevier Science Publishers B. V., 1990.

[55] A. R. Conway and X. Xiao, *Fatigue of Composite Materials*, vol. 3 of *American Society for Composites Series*, ch. Progressive fatigue damage modeling in CFRP laminates using an ABAQUS UMAT approach. DEStech Publications, Inc, 2012.

[56] I. Lapczyk and J. Hurtado, "Progressive damage modeling in fiber-reinforced materials," 2006.